Journal of Power Sources 236 (2013) 321–340

Contents lists available at SciVerse ScienceDirect

Journal of Power Sources

journal homepage: www.elsevier.com/locate/jpowsour

A computationally efficient hybrid 3D analytic-numerical approach for modelling species transport in a proton exchange membrane fuel cell

G. Tavčar*, T. Katrašnik

University of Ljubljana, Faculty of Mechanical Engineering, Aškerčeva 6, SI-1000 Ljubljana, Slovenia

HIGHLIGHTS

- ► Computationally fast hybrid 3D species transport model in fuel cells is presented.
- ► Model is 1D numerical in direction of flow and 2D analytic in other two dimensions.
- ► Model validation showed high accuracy of 3D species concentration distribution.
- ► Due to its analytic part its computational times are comparable to 1D models.
- ► High accuracy and computational efficiency make it a promising system level tool.

ARTICLE INFO

Article history:
Received 2 August 2012
Received in revised form
16 December 2012
Accepted 21 January 2013
Available online 30 January 2013

Keywords:
Fuel cells
Species transport
Analytic modelling
Numerical modelling

ABSTRACT

This paper presents an innovative hybrid analytic-numerical approach to modelling species transport in fuel cells suitable for application on the system level. The core principle of this modelling approach is taking 1D numerical model for gas-flow and superimposing onto it a 2D analytic solution for concentration distribution in the plane perpendicular to the gas-flow together giving a 3D information on species concentration in the fuel cell. A hybrid analytic numerical model of a simple geometry isothermal fuel cell is presented and comparatively evaluated by benchmarking it against a professional full 3D CFD simulation tool. This evaluation shows very close agreement with the benchmarking 3D CFD simulation and computational times comparable to 1D models. This computational efficiency originates in the model's analytic nature in the other two dimensions making it suitable for system level application. The paper features an extensive appendix with a comprehensive detailed mathematical derivation of the hybrid analytic-numerical model.

1. Introduction

Fuel cells embedded in dynamic systems such as road vehicles are subjected to varying loads that require operation at a wide range of operational points. Development of fuel cells for such systems thus also involves optimisation of the whole system which requires, in addition to the detailed analyses of specific components of the system, also the analyses on the system level. Such analyses are normally performed during the early development stages when experimental data are not yet available. This calls for predictable system level fuel cell computer models. Additionally, to be able to perform numerous simulations with high fidelity at these development stages, also high computational speeds at minimal trade off with accuracy of the model are strived for.

A great number of fuel cell models can be found in the literature and some are also available as packages in commercial software. Their approaches to modelling the fuel cell behaviour are different and can be categorised according to:

- The approach to describing physical phenomena i.e.: Analytic, mechanistic, semi empirical, fully empirical;
- Their dimensionality: 0D, 1D, 2D, quasi 3D, 3D;

Comprehensive overviews of the various approaches to fuel cell (FC) modelling are given by Cheddie et al. [1] and Haraldsson et al. [2].

0D FC models are usually analytic highly simplified models operating only on integral variables. They lack any spatial resolution that is curtail for modelling fuel cells that are highly nonlinear systems and are thus useful for quick and approximate calculations for simple systems. Examples: Usman Iftikhar et al. [3], Tirnovan et al. [4], Xue et al. [5].

* Corresponding author. Tel.: +386 1 4771 310.
E-mail addresses: gregor.tavcar@fs.uni-lj.si, gregor.tavcar@gmail.com (G. Tavčar).

0378-7753/$ – see front matter © 2013 Elsevier B.V. All rights reserved.
http://dx.doi.org/10.1016/j.jpowsour.2013.01.136

1D FC models gain higher accuracy by calculating also the variation of variables along the direction of gas flow. However, they cannot properly account for the concentration gradients in directions perpendicular to the fuel cell membrane since they lack resolution in that perpendicular dimension. The membrane water content, crucial for fuel cell performance, is affected by water transport into and out of the membrane which is driven by these concentration gradients. This means 1D models cannot adequately deal with one of the physical phenomena greatly affecting fuel cell performance. Examples: Springer et al. [6], Wohr et al. [7], Maggio et al. [8], Gurau et al. [9].

2D FC models additionally feature exactly that dimension perpendicular to the membrane which makes them highly accurate, since the remaining unaccounted for dimension that is perpendicular to the flow direction and parallel to the membrane bears much less importance to the fuel cell performance. Although highly accurate 2D models feature too long computational times to be suitable for system level simulations. Examples: Baschuk et al. [10], Rajani et al. [11], Khakbaz Baboli et al. [12].

Full 3D CFD models that are usually semi empirical models are the most accurate. Their accuracy comes at high cost of requiring a lot of computational time and memory space. Examples of 3D & quasi 3D: Meng [13], Sivertsen et al. [14], Vath et al. [15], Al-Baghdadi et al. [16], Mueller et al. [17].

In addition to the aforementioned models that are based on different levels of physical modelling in various dimensionalities there are also purely empirical data driven models that are calibrated by performance values on a set of operational points that are either measured or obtained by higher fidelity models. These empirical models are both accurate and very fast but they lack any predictability and typically fail at operational points beyond the field of calibration. Moreover, they are always characteristic to only one specific system, which limits their use in the development process. Examples: Tirnovan et al. [18], Hatti et al. [19].

The fundamental difference between 1D and 3D approach illustrates Fig. 1. Bearing no information on the concentration distribution in cross-sectional plane the 1D model in B suffers from inability to accurately treat the concentration gradient induced diffusive species transport from the membrane. The 3D approach in A on the other hand captures the concentration distribution, the concentration gradients and consequent diffusive species transport in all spatial directions.

As an improved, computationally quick and yet accurate model for species transport in fuel cells suitable for use on the system level this article proposes and describes a Hybrid Analytic Numerical quasi 3D approach (HAN). The main principle behind HAN model is superimposing a 2D analytic solution for the plane perpendicular to the gas-flow onto the 1D numerical model for the flow along the channel. This is computationally efficient since the calculation of 2D analytic solution adds to the 1D model additional computational load that is of the same order of magnitude as the computational load of the base 1D calculation.

Overall HAN modelling approach shows the following advantages:

- achieving higher accuracy than 1D models due to its 3D nature,
- not being considerably slower than 1D models due to being analytic in the other two dimensions

The HAN model does not strive to compete with full 3D CFD detailed models but rather aims at upgrading 1D modelling approach and thus positions itself as an advanced system level tool. The presented HAN model is aimed for modelling species transport in the fuel cells, which crucially influences the performance of the fuel cell. The paper therefore outlines the modelling approach in Section 2 and governing equations of the species transport in Section 3. The accuracy of the species transport modelled by HAN is benchmarked with the results obtained by a professional 3D CFD tool. The simulation setup is introduced in Section 4, in Section 5 results and their analysis is provided and Section 6 summarised the main conclusions. Detailed mathematical derivation of the model is given in Appendix.

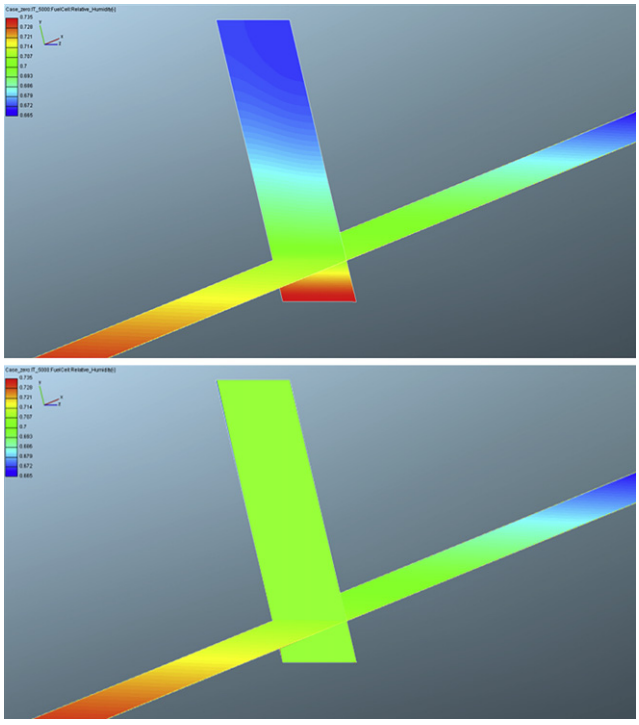

Fig. 1. Relative humidity in channel as calculated by (a) 3D and (b) 1D approach to fuel cell modelling. The strip stretching from right to bottom left is shows distribution of relative humidity along the channel length in a plane parallel to membrane, the rectangle perpendicular to this strip shows the distribution over the cross section of the channel.

2. The modelled fuel cell

To illustratively demonstrate the principle of this hybrid analytic-numerical approach a simple proton exchange membrane fuel cell has been modelled. The topology and geometry of the fuel cell model as illustrated in Fig. 2 are as follows: it is a straight, co-flow, hydrogen–oxygen type PEM fuel cell (FC) comprising the following sub-elements: channel for oxygen delivery, oxygen-side gas diffusion layer (GDL), thin catalyst layer for oxygen reduction, hydrated proton exchange membrane, thin catalyst layer for hydrogen oxidation, hydrogen-side GDL, channel for hydrogen delivery. This simple FC geometry enables a very transparent comparison of results calculated by HAN to the results calculated with high fidelity 3D CFD model which is necessary for validation of the HAN.

The derivation of HAN is based on the following assumptions:

I. A steady state solution of the problem is sought.
II. The problem is isothermal meaning a constant uniform temperature is assumed for the whole fuel cell and no energy equation is calculated.
III. The gasses are treated as ideal.
IV. There is no liquid water in GDLs and Channels.
V. The diffusion constants are pressure insensitive. This is justifiable due to very small pressure variations in the fuel cell owing to the very simple geometry. (See pressure data in Results)

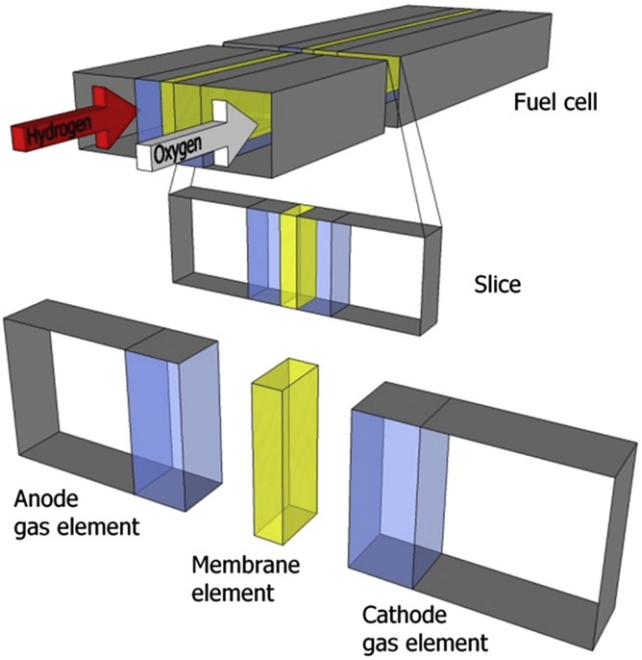

Fig. 2. Schematic of modelled fuel cell. Grey surfaces represent the walls, translucent blue region the GDLs and the translucent yellow the membrane. (For interpretation of the references to colour in this figure legend, the reader is referred to the web version of this article.)

VI. The diffusion system is always bi-componential (either oxygen and water vapour or hydrogen and water vapour) and thus described by a scalar diffusion constant.
VII. The effective (macroscopic) diffusion constant used in GDL is the diffusion constant for empty space (which applies in the channel) divided by the tortuosity of GDL.
VIII. Diffusion in gas in the direction of gas-flow is neglected. In this direction the diffusive species transport is 3–4 orders of magnitude smaller than the dominant convective transport (see Results)
IX. Diffusion of water within the membrane is only in the direction perpendicular to the membrane sheet. This is due to the thinness of the membrane resulting in negligible concentration gradients in the plane of membrane compared to the gradients across the membrane. Same assumption makes the benchmark CFD programme. Also the molar flux of water, physically a vector, on the membrane/gas element interface is also assumed to be only in this direction.
X. There is no convective transport in GDL. The very small pressure variations produce only negligible convective flow in the GDL. (See Fig. 7 in Section 5)
XI. At the membrane/gas boundary the membrane water content is in equilibrium with water vapour concentration in the gas (i.e. at this boundary the water activity in membrane is equal to the water activity in gas).
XII. The flow in channels is laminar and the velocity has no components perpendicular to the direction along the channel.
XIII. The proton flow across the membrane is taken as a parameter defined by the current density calculated by any fuel cell sub model dealing with electrochemistry.
XIV. The membrane assumes no gas crossover. Thus the only species transported through the membrane besides protons is water.
XV. The membrane water diffusion constant is independent to the membrane water content. Many aforementioned models treat this diffusion constant as a function of water content; however this function found in Refs. [15,20] or [21], differs significantly from the one found in Refs. [6,17] or [10] and from the constant value found in Ref. [11] or [22]. Therefore there seems to be no general agreement on what this function is justifying the choice of independent diffusion constant.

These assumptions are all within the sets of usual assumptions made by other models of comparable modelling depth presented in the Introduction. HAN assumes coupling with any electrochemistry model that calculates the distribution of the current density. The objective of this paper is to present and evaluate HAN's capability to accurately model species transport. As the comparative evaluation of HAN was done with a 3D CFD model it is also required that boundary conditions that drive the species transport are as identical as possible. Therefore in this particular case the current density calculated by the 3D CFD model was also taken as the boundary condition of the HAN, whereas when HAN is run as the stand alone simulation it uses its own electrochemistry model.

3. Governing equations

The term "hybrid analytic-numerical quasi-3D" means that the equations governing the distribution of species concentrations are resolved analytically in the 2D plane that is perpendicular to the gas flow and numerically in the other remaining direction, the direction of the gas flow. The bulk gas flow is essentially treated as 1D flow with superimposed simple 2D velocity profile of laminar flow and 2D species concentration profile.

The fuel cell is sliced along the direction of gas flow into a number of slices as depicted in Fig. 2. Each slice is treated as a 2D object meaning that only variation of variables in the plane perpendicular to gas flow is addressed. The transport of species and the consequential distribution of concentrations are, within each element, regarded as being governed solely by the diffusion equation as described in the Subsection 3.1.

The bulk gas flow is treated as 1D phenomenon defined by the variables of pressure, mean velocity and molar composition. Their variation from one slice to the next downstream slice is, for each of the two gas flows, calculated by the 1D mass and momentum equations described in the Subsection 3.2.

The analytic solutions for the consecutive slices are coupled via the source/sink terms in the sense that what exits one enters the other taking into account also the changes in the bulk gas flow. Due to assumptions VIII, IX and X there is no exchange of species between slices in the regions of the membrane and GDLs but only along the channels so the source and sink term are nonzero only for channel region as depicted in Fig. 3. The calculation procedure for obtaining a solution for the whole fuel cell as a series of consecutive solutions for all the slices is presented in Subsection 3.3.

3.1. 2D solutions for slices

To treat the water transport in gaseous phase in channels and GDLs and in liquid phase in the membrane each slice is further divided into three elements: two gas elements (a cathode and an anode gas element; see Fig. 3) and a membrane element between the two (see Fig. 4). Each element is treated as a 2D object meaning that there is no variation of any variable along the direction of gas flow within that element. The solution for each slice is constructed by coupling the partial solutions for each of the two gas elements via the membrane element.

3.1.1. Gas element

The species transport in ideal gas is modelled by Stefan–Maxwell diffusion equations which, for a general case of gas

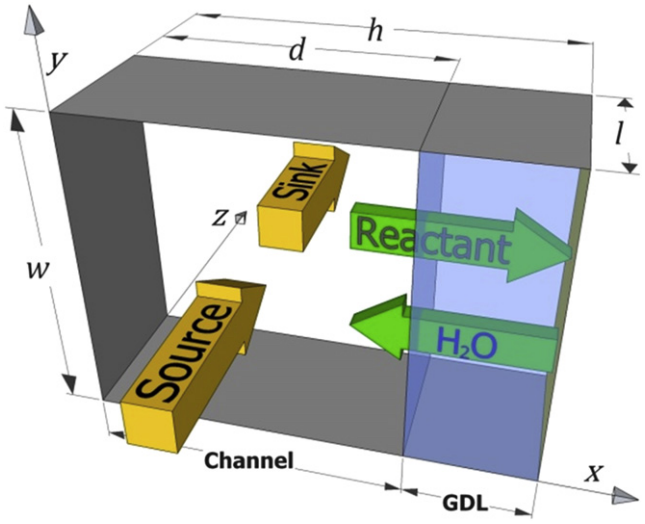

Fig. 3. Schematic of a gas element. The grey surfaces are the walls where the boundary condition requires zero concentration gradient normal to boundary, yellowish surface is the gas/membrane interface and the boundary condition is the diffusive flux of species, translucent blue surface penetrated by the green arrows is the channel/GDL interface requiring continuity of species flux. The source and the sink are convective inflow of species from previous element upstream and outflow into the next element downstream respectively. (For interpretation of the references to colour in this figure legend, the reader is referred to the web version of this article.)

mixtures with n components (numbered with i running from 1 to n), read [23]:

$$\nabla c_i = \sum_{\substack{j=1 \\ j\neq i}}^{n} \frac{c_i c_j}{c_0 D_{ij}} \left(\frac{\boldsymbol{j}_j}{c_j} - \frac{\boldsymbol{j}_i}{c_i} \right), \tag{1}$$

where D_{ij} is the binary diffusion coefficient for the binary solution of the components i and j, vector $\boldsymbol{j}_i$ is the molar flux of the component i, c_i is the corresponding molar concentration and $c_0 = \sum_{i=1}^{n} c_i$ is the total molar concentration. For the special case of binary gas mixtures (i.e. bi-componential diffusion systems as assumed in VI) the Maxwell diffusion equations reduce to the following two diffusion equations [23]:

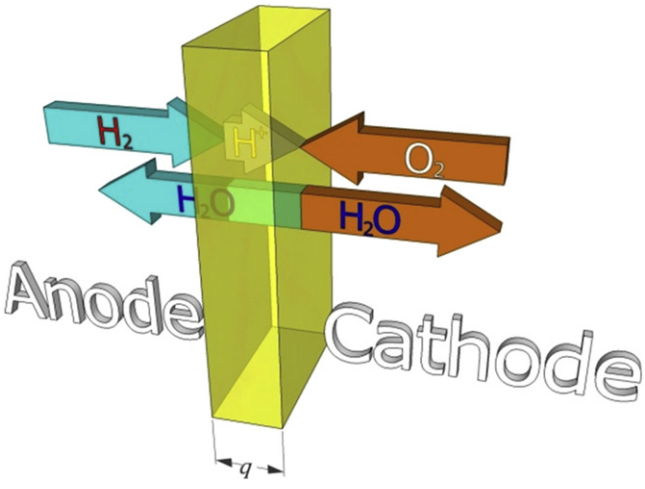

Fig. 4. Schematic of species transport in membrane. The yellow region represents the membrane, the blue arrows represent the species transport from/to the anode gas element and the brown arrows the species transport from/to cathode gas element, the grey arrow represents the proton flow across the membrane. (For interpretation of the references to colour in this figure legend, the reader is referred to the web version of this article.)

$$\boldsymbol{j}_1 = \boldsymbol{v} c_1 - D \nabla c_1, \tag{2}$$

$$\boldsymbol{j}_2 = \boldsymbol{v} c_2 - D \nabla c_2, \tag{3}$$

where $\boldsymbol{v}$ is the net molar velocity of the gas and $D = D_{12}$ is the binary diffusion coefficient for the binary solution of the two components. For the case of constant temperature T (assumption II) and constant pressure p (within a gas element the pressure is treated as constant) the total molar concentration $c_0 = p/RT$ is also constant. This means that for finding the distribution of concentrations c_1 and c_2 it suffices to solve only Equation (2) since the distribution of the other concentration is obtained by:

$$c_2 = c_0 - c_1. \tag{4}$$

Thus, the following derivation of governing equations for gas element shall deal only with the concentration of water vapour.

The steady state solution requires that:

$$\frac{\partial c}{\partial t} = -\nabla \cdot \boldsymbol{j} = D \nabla^2 c - \nabla \cdot (\boldsymbol{v} c) = 0, \tag{5}$$

where c is the molar concentration of water vapour and $\boldsymbol{j}$ its molar flux. Following assumption VIII there is no diffusive transport along the z coordinate and thus the term $D\partial^2 c/\partial z^2$ is neglected. Following assumptions X and XII there are no components of $\boldsymbol{v}$ along x and y coordinates. This simplifies the Equation (5) to:

$$\frac{\partial c}{\partial t} = D \nabla^2 c - \frac{\partial (\boldsymbol{v} c)}{\partial z} = 0, \tag{6}$$

where $v = v_z = |\boldsymbol{v}|$ is the z component of $\boldsymbol{v}$ and at the same time also its absolute value and $\nabla^2 = \partial_x^2 + \partial_y^2$ is the Laplace operator in the xy plane. Furthermore, the numerical treatment of the gas flow along z coordinate uses the following finite-difference approximation for the derivative $\partial_z(v\, c)$:

$$\frac{\partial (\boldsymbol{v} c)}{\partial z} \cong \frac{1}{l} \left((\boldsymbol{v} c)|_{z=z_{\text{exit}}} - (\boldsymbol{v} c)|_{z=z_{\text{enter}}} \right), \tag{7}$$

where $l = z_{\text{exit}} - z_{\text{enter}}$ is the depth of slice with z_{enter} and z_{exit} denoting the value of z coordinate at the point where the gas flow enters and exits the gas element respectively. Equation (7) can, from the point of view of the diffusion in a single gas element, also be interpreted as following: The term $1/l(\boldsymbol{v} c)|_{z=z_{\text{enter}}}$ is the species inflow contribution i.e. the *source* term and $1/l(\boldsymbol{v} c)|_{z=z_{\text{exit}}}$ is the species outflow contribution i.e. the *sink* term.

This enables treating both convective and diffusive phenomena within a gas element with a single 2D diffusion equation:

$$\frac{\partial c(x,y)}{\partial t} = D \nabla^2 c(x,y) + s^{\text{src}}(x,y) - s^{\text{snk}}(x,y) = 0, \tag{8}$$

where, depending on the region, D takes on the following values $D^{\text{O}}_{\text{chnl}}$, $D^{\text{O}}_{\text{GDL}}$, $D^{\text{H}}_{\text{chnl}}$, and $D^{\text{H}}_{\text{GDL}}$ which are the diffusion constants of: water vapour/oxygen system in the channel and GDL and water vapour/hydrogen system in the channel and GDL respectively. Due to assumptions II, V and VI these four diffusion constants are scalars and they apply along the whole fuel cell. The source and sink term, schematically represented by the yellow arrows in Fig. 3, are expressed as:

$$s^{\mathrm{src}}(x,y) = \frac{1}{l} v_{\mathrm{pr}}(x,y) c_{\mathrm{pr}}(x,y), \tag{9}$$

$$s^{\mathrm{snk}}(x,y) = \frac{1}{l} v(x,y) c(x,y), \tag{10}$$

where and $v(x,y)$ is the velocity profile, with subscript pr denoting the value from previous element i.e. the neighbour element upstream the gas flow. The velocity profile in Equation (9) and (10) always has the same dome-like shape of laminar flow (see Fig. 7) that is scaled with the average velocity in the channel of the element in question:

$$v(x,y) = \tilde{v}\, u(x,y), \tag{11}$$

where u $(x,\ y)$ is the unit-less dome shape and $\tilde{v}$ the average velocity. Derivation of the velocity profile is given in Appendix B.

The diffusive flux of species between the membrane and the gas, schematically represented with green arrows in Fig. 3, serves as boundary condition. Since due to assumption XIV the water is the only species diffusing from membrane this boundary condition can be expressed as:

$$\kappa D_{\mathrm{GDL}} \frac{\partial c(x,y)}{\partial x}\bigg|_{x=h} = j(y), \tag{12}$$

where κ is volume fraction of the gaseous phase in the GDL, $x = h$ denotes the position at the GDL/membrane boundary and j molar flux of water entering the gas element at the membrane/GDL boundary. In the anode gas element $j(y)$ can also be negative. This occurs in cases where the electroosmotic pull of proton flow is stronger than back diffusion. In these cases the green arrow indicating the water flow into the gas element in Fig. 3 points into the opposite direction. Since there is no flux through walls other boundary conditions are:

$$\frac{\partial c(x,y)}{\partial n}\bigg|_{\mathrm{wall}} = 0, \tag{13}$$

where n denotes the coordinate normal to the boundary. Additionally, the continuity of species flow imposes the following condition for the channel/GDL boundary:

$$D_{\mathrm{chnl}} \frac{\partial c(x,y)}{\partial x}\bigg|_{x=d^-} = \kappa D_{\mathrm{GDL}} \frac{\partial c(x,y)}{\partial x}\bigg|_{x=d^+}, \tag{14}$$

where $x = d^-$ and $x = d^+$ denote the position at the channel/GDL interface on the channel side and GDL side respectively.

Within every gas element the 2D analytic partial solution of the species concentration distribution comes in a form of a linear combination of eigen functions of the $D\nabla^2$ operator. There are two families of eigen functions, both defined in Appendix A: the first, defined by Equation (A15), deals with convective transport and the second, defined by Equation (A26), deals with the diffusion from membrane. The definition region of all these eigen functions, also called harmonics, comprises the cross-sectional area of both the channel and the adjacent GDL taking into account the different material properties of the two regions. The harmonics are, because they are two-dimensional, generally indexed with a double index m, n reflecting the number of modes in y and x direction. For computational feasibility a limited number of harmonics is taken into account by defining M, N as the maximal values of m, n.

The partial solution for a gas element, represented by Equation (A80) in Appendix A, is obtained by treating the source term, diffusion from membrane and average velocity of gas flow as input parameters. The full derivation is given in Subsection A.1 of Appendix A.

3.1.2. Membrane element

The boundary conditions of the two gas sides are coupled via the membrane model and the species consumption/production at the catalyst that are defined by the assumed current density taken from a separate electrochemistry sub-model (the CFD simulation in presented case). The membrane model calculates water transport across the membrane driven by the electroosmotic drag of proton flow and the back diffusion of water. Due to the assumption IX each membrane element only interacts with the two gas elements on each side and not with the other neighbour membrane elements.

The water is produced on the cathode catalyst and it diffuses away into the cathode gas element and through the membrane into the anode gas element. In steady state this requires that:

$$j_{\mathrm{O}}(y) + j_{\mathrm{H}}(y) = \frac{i(y)}{2F}, \tag{15}$$

where j_{O} and j_{H} are the molar flux of water into cathode and anode gas element respectively, $i(y)$ is the electric/proton current density and F is the Faraday constant. Since all water is produced on the cathode catalyst the molar flux of water traversing the membrane j_{mmb} is, in steady state, equal to the molar flux of water entering anode gas element j_{H} (as depicted in Fig. 4). In cases where the electroosmotic pull of proton flow is stronger than back diffusion j_{H} is negative and the blue arrow indicating the water flow into the anode in Fig. 4 points into the opposite direction. Due to the assumption IX the molar flux of water through the membrane is treated as a scalar. The molar flux of water through the membrane has two driving forces: the diffusive flux due to the concentration gradient and the electroosmotic drag of protons:

$$j_{\mathrm{mmb}}(y) = j_{\mathrm{H}}(y) = D_{\mathrm{mmb}} \frac{\left(\Lambda^{\mathrm{O}}(y) - \Lambda^{\mathrm{H}}(y)\right)}{q} - n_{\mathrm{drg}} \frac{i(y)}{F}, \tag{16}$$

Where D_{mmb} is the diffusion constants of water in membrane, Λ^{O} and Λ^{H} are the membrane water content at the element/membrane boundary on the cathode and anode side respectively, q is the membrane thickness and n_{drg} is the average number of water molecules each proton drags with it. When in equilibrium, the membrane water content Λ is a nonlinear function of the relative humidity of the surrounding gas. The empiric polynomial formula from Springer et al. [6] is used:

$$\Lambda = \Lambda(\mathrm{Rh}) = 0.043 + 17.8\,\mathrm{Rh} + 39.85\,\mathrm{Rh}^2 + 36\,\mathrm{Rh}^3. \tag{17}$$

Due to the isothermal conditions in assumption II the water vapour concentration c is a proportional measure of relative humidity:

$$\mathrm{Rh}(x,y) = \frac{c(x,y)}{c_{\mathrm{sat}}} = c(x,y) \frac{RT}{p_{\mathrm{sat}}}, \tag{18}$$

where p_{sat} is the saturated vapour pressure at temperature T and R is the gas constant. This means that membrane water content is, in equilibrium, directly related to water vapour concentration, i.e. $\Lambda = \Lambda(c)$. Denoting the concentrations of water vapour in cathode and anode gas element with c_{O} and c_{H} respectively and defining $\zeta^{\mathrm{O}}(y) = c_{\mathrm{O}}(x = h, y)$ and $\zeta^{\mathrm{H}}(y) = c_{\mathrm{H}}(x = h, y)$, the boundary conditions at the two boundaries with gas elements are thus expressed as:

$$\Lambda^{O}(y) = \Lambda\left(\zeta^{O}(y)\right), \quad \Lambda^{H}(y) = \Lambda\left(\zeta^{H}(y)\right). \tag{19}$$

The difference in membrane water content in Equation (16) can be expressed as:

$$\Lambda^{O}(y) - \Lambda^{H}(y) = \chi \cdot \left(\zeta^{O}(y) - \zeta^{H}(y)\right), \tag{20}$$

where $\chi = \chi(\zeta^{O}, \zeta^{H})$ is a nonlinear function of ζ^{O} and ζ^{H}:

$$\chi\left(\zeta^{O}, \zeta^{H}\right) = \frac{\Lambda\left(\zeta^{O}\right) - \Lambda\left(\zeta^{H}\right)}{\zeta^{O} - \zeta^{H}}. \tag{21}$$

From mathematical point of view the latter two definitions are redundant, however they are useful for computational purposes. Namely, the whole set of coupled linear equations for obtaining concentration distributions on the anode and the cathode side (given in Subsection A.3 of Appendix A) is solved by using expression (20) in Equation (16) and assuming χ to be a parameter (i.e. $\chi \neq \chi(\zeta^{O}, \zeta^{H})$). The resulting concentration distributions are than used to recalculate χ according to Equations (17), (18) and (21) and the linear equations are solved again, this time with the new value of χ. This procedure is, together with the calculations of 1D gas-flow described in the next section, iterated till sufficient convergence (outlined in the flowchart in Fig. 5). Equations (15), (16) and (20) couple the two partial solutions for the two gas elements resulting in the set of Equation (A93) in Appendix A. The full derivation is given in Subsection A.2 of Appendix A.

3.2. 1D gas-flow

The partial solution for a gas element crucially relies on the information on the average velocity $\tilde{v}$ of the gas flow in the channel part of the gas element. This average velocity is calculated by the 1D inviscid flow steady state momentum equation for the channel region. The momentum equation embodies the requirement that the resultant force acting on the control volume of the short section of the channel equals the difference between the linear momentum flux into the control volume and the linear momentum flux out of it i.e. the change in linear momentum flux $\Delta\dot{L}$ across the length of the channel section [24]. The resultant force on the control volume is the sum of the net pressure force resulting from the pressure difference Δp across the length of the channel section and the net friction force F_{fr} resulting from the friction between the gas flow and channel walls. $\Delta\dot{L}$ and F_{fr} are given by Equations (A96) and (A100) respectively in Subsection A.4 of Appendix A. The momentum equation thus reads:

$$-A\,\Delta p + F_{fr} = \Delta\dot{L}, \tag{22}$$

where A is the cross-sectional area of the channel. The upper Equation (22) is solved using the ideal gas equation in the form:

$$p\tilde{v}A = \dot{n}RT, \tag{23}$$

where p is the pressure, $\dot{n}$ the net molar flux of gas and T the temperature. The full solution for $\tilde{v}$ is given by Equation (A102) in Appendix A and its derivation is presented in Subsection A.4 of Appendix A.

3.3. Solution for whole fuel cell

The steady state solution for the complete fuel cell is made of consecutive steady state solutions for each slice. Each gas element is, within the slice, coupled via the membrane to the adjacent gas element on the other side of the membrane as depicted in Fig. 2. Additionally each gas element is via the source term coupled to the gas element on the same side of the membrane in the neighbour slice upstream the gas flow as depicted in Fig. 3 (the source term of the element in question being the sink term of the upstream neighbour element as indicated in the left orange box in Fig. 5). As mentioned in Subsection 3.1.1 the analytic partial solutions for gas elements are treated as a two series of (in general non orthogonal) eigen functions, i.e. series vectors. The derivation of the two families of eigen functions and the algebraic manipulation for obtaining the series vectors is given in Appendix A. Since both families of eigen functions are the same for all gas elements on one side (cathode or anode side) the coupling of the partial solution for one gas element with the partial solution for its upstream neighbour gas element via the source term is done on the level of coupling the components of the corresponding series vectors as done by Equation (A80). The definitions of families of eigen functions (defined by Equations (A15) and (A26) together with

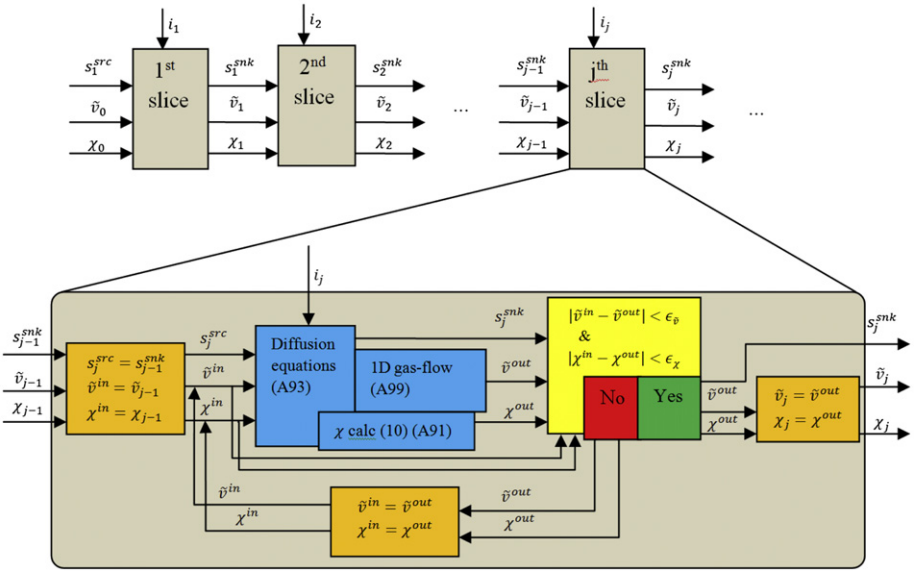

Fig. 5. Flowchart of HAN calculation procedure for the whole fuel cell and for each slice. i_j denotes the current density in the jth element. Here s^{src}, s^{snk} and $\tilde{v}$ are to be understood as representing the values for both cathode and anode side.

Appendix C and Appendix D) also contain the diffusion constants which are different for anode side and for cathode side, therefore the two families of eigen functions for cathode gas elements and the two families for anode gas elements are not the same. However, the values of all these eigen functions at the membrane form a family of functions that is the same for both cathode and anode side which again enables coupling of the partial solutions for the anode and cathode gas element on the level of coupling the components of the corresponding series vectors. This coupling of series vectors requires only algebraic manipulation meaning that solving the governing equations for the anode and cathode gas elements and the membrane element results in a set of simple algebraic Equation (A93) given in Subsection A.3 of Appendix A.

The information on average velocity $\tilde{v}$ is required for calculating the solutions for slices with the aforementioned set of Equation (A93) and also vice versa: The information on net water inflow obtained from Equation (A93) is required for calculating the average velocity $\tilde{v}$ that is calculated by solving Equations (22) and (23) resulting in Equation (A102) given in subsection A.4 of Appendix A. Because Equation (A102) is nonlinear the calculation of Equations (A93) and (A102) is done in an iterative routine with some initial approximation for $\tilde{v}$ as represented in the flowchart in Fig. 5.Additionally this iterative routine also makes the nonlinear calculations in the membrane. This is done by iteratively correcting the constant χ in Equation (20) by recalculating χ according to definition (A91) using the nonlinear Equation (17) and Equations (18) and (21). The calculations done iteratively are represented by blue boxes in Fig. 5. After each iteration the sufficiency of convergence is assessed as represented by the yellow box in Fig. 5.

The calculation of $\tilde{v}$ in Equation (A102) also provides information on the pressure drop. If necessary, the routine for the whole fuel cell is iterated adjusting inlet pressure to get the desired outlet pressure. This iterative calculation of the whole fuel cell routine would be necessary in case of counter flow design. By finding appropriate eigen functions or splitting them onto multiple domains HAN approach can be also used for modelling more complex fuel cell geometries with parallel channel arrangement where the gas at each electrode flows in only one direction. For serpentine gas channel geometries with significant gas-flow through the GDL in direction perpendicular to the direction of gas-flow in channels a further extension of the HAN model is needed to adequately treat also the source and sink terms in direction perpendicular to gas-flow in channels.

4. Simulation setup

This section summarises the parameters used for setup of the CFD and HAN simulation models. To ensure credibility of the CFD results the computational fluid dynamics software used was AVL FIRE® v2011 with the "Fuel cell" module which has been validated on physical fuel cells found in Refs. [25,26].

4.1. 3D CFD

The aforementioned fuel cell module allows user defined meshing of the channel and GDL and treats the two catalyst layers as zero-thickness surfaces sandwiching the membrane that is sectioned in such a way that it always contains 12 slices between the two catalyst surfaces. The species transport in membrane is, due to its' thinness, assumed to have only the component perpendicular to the plane of membrane.

The meshing of the channels and GDLs of the fuel cell shown in Fig. 6 was done as follows: The anode and the cathode side meshes are treated equally and are mirror images of each other. Due to symmetry across y–z plane only one half of the fuel cell was

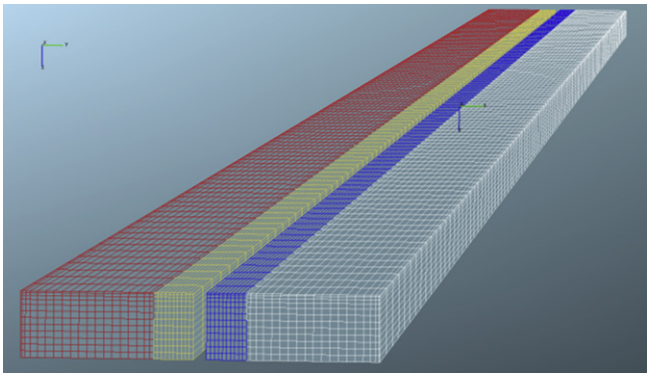

Fig. 6. CFD fuel cell mesh white part of the mesh is the cathode channel, blue the cathode GDL, yellow the anode GDL and red the anode channel. (For interpretation of the references to colour in this figure legend, the reader is referred to the web version of this article.)

simulated. The so obtained half of the channel measuring 1.0 mm × 0.5 mm × 70.0 mm is sectioned into 19 × 12 × 100 sections and the 0.3 mm × 0.5 mm × 70 mm half of GDL into 10 × 12 × 100 sections.

The gas composition was, according to assumption VI, taken as bi-componential, i.e.: H_2 with $H_2O_{(g)}$ for the anode and O_2 with $H_2O_{(g)}$ for cathode. The amount of water vapour in the gases at inlets was defined by the relative humidity of the feed gas boundary condition setting. The parameters for membrane assumed no gas crossover. The isothermal conditions were ensured by excluding calculation of energy equation in the CFD solver setup.

For purposes of HAN calibration two simulations were run, one with gas velocity at inlet (for both cathode and anode) of 0.2 m s^{-1} and one with 0.3 m s^{-1}. Other boundary conditions were same for both: the ambient pressure (100 kPa) at outlets, fixed potential difference between cathode and anode 0.60 V, Temperature 350 K and relative humidity of 30% at both inlets. This low relative humidity was chosen to test the HAN model at large concentration gradients and large span of concentration values.

4.2. HAN

The programming environment used for HAN was Wolfram Mathematica 8.0. In the HAN model the fuel cell was also sliced into 100 sections along the direction of gas flow and the number of harmonics taken into account was 15 with 3 modes in y coordinate and 5 in x coordinate (this means $M = 2, N = 4$ since indexing starts with 0). Additionally a case with 100 harmonics (i.e. $M = 9, N = 9$) was examined to see what influence the number of harmonics has on the accuracy and calculation times. For evaluation of computational efficiency also a case with only first harmonic (i.e. $M = 0, N = 0$) was run to simulate a purely 1D model. The same gas composition assumptions and same boundary conditions as for CFD were applied (with the exception of cathode to anode potential that does not apply in the case of HAN). The current density data obtained from the CFD results in form of 12 × 100 discrete values was split among the 100 slices and within each slice the 12 values converted to the M number of harmonics according to definition (A84) in A.2 of Appendix A. The calibration was done by only varying the n_{drg} parameter in Equation (16). All other parameters such as diffusion constants were set to identical values as in the CFD model.

5. Results

In this section the comparative results of HAN and CFD simulation are presented. The two solutions for inlet gas velocities of 0.2 m s^{-1} and 0.3 m s^{-1} obtained by HAN were evaluated at the

same points as the CFD simulations and the following equation for evaluating agreement between CFD and HAN was used:

$$\mathrm{dev} = \sqrt{\frac{\sum_{i=1}^{n_{\mathrm{all}}}\left(c^i_{\mathrm{HAN},0.2} - c^i_{\mathrm{CFD},0.2}\right)^2 + \sum_{i=1}^{n_{\mathrm{all}}}\left(c^i_{\mathrm{HAN},0.3} - c^i_{\mathrm{CFD},0.3}\right)^2}{2n_{\mathrm{all}}}}, \tag{24}$$

where index i runs over all calculation elements of the CFD simulation ($n_{\mathrm{all}} = 46{,}000$), the subscripts 0.2 and 0.3 denote the two cases with different inlet gas velocities. By varying n_{drg} the minimum of dev was sought and found at $n_{\mathrm{drg}} = 1.07$, dev = 0.006. When calibrating with only the solution for one inlet gas velocities the minimum was found at $n_{\mathrm{drg}} = 1.06$ for 0.2 m s^{-1} and $n_{\mathrm{drg}} = 1.09$ for 0.3 m s^{-1}. The fact that the obtained best-fit values for different calibrations vary only little shows a wider validity and predictability of the model.

5.1. Sectional profiles

In Figs. 7–12 all plots that are coloured green show the values as calculated by the CFD simulation whereas the ones coloured purple show the values as calculated by the HAN with 15 harmonics. Additionally, yellow is used for a plot of HAN with 100 harmonics. The coordinate system in the plots is oriented so that the yz plane at $x = 0$ is in the middle of the membrane and the cathode side is at $x > 0$ and anode side at $x < 0$. Due to symmetry always only half of the fuel cell is plotted.

Fig. 7(a) shows the z component of velocity profile $v(x, y)$ on the cross section of anode as calculated by the CFD simulation. It is evident that the velocity in the GDL is negligible. The maximal velocity anywhere in GDL and the maximal value of x or y component of velocity are less than 1% of the average velocity in the channel, justifying the assumptions X and XII.

Fig. 7(b and c) shows the plot of $v(x, y)$ as seen by HAN (again, these are plots of the z component of velocity, since due to assumptions X and XII the velocity as seen by HAN has no other components). The two differ in the number of eigen functions (i.e. harmonics) taken into account. This comparison is illustrative of how higher number of harmonics results in higher accuracy, especially when comparing how well the two reproduce the sharp boundary between channel and GDL. The fact that the velocity profile as seen by HAN is not exactly zero on the whole GDL region is inherent to the harmonics being defined on the domain comprising both the channel and the GDL regions. However, as discussed at the end of this section, this proves not to be a significant source of error.

The water vapour concentration is presented in terms of relative humidity (according to Equation (18)), whereas the concentration of reactant c_r is presented in terms of molar fraction mfr defined according to Equation (4) as:

$$\mathrm{mfr} = \frac{c_r}{c_0} = 1 - \frac{c}{c_0}, \tag{25}$$

In Figs. 9, 11 and 12 the relative humidity equivalent in the membrane is obtained from Equation (18) and (20) as follows:

$$\mathrm{Rh}_{\mathrm{mmb}} = \frac{\Lambda}{\chi}\frac{RT}{p_{\mathrm{sat}}}, \tag{26}$$

Fig. 9 shows two views of a comparative plot of distribution of relative humidity on the symmetry plane of the fuel cell (red section plane in Fig. 8). The gasses enter the fuel cell at $z = 0$ and exit at $z = 70$ mm. It shows increasing relative humidity on cathode side ($x > 0$) and decreasing relative humidity on anode side ($x < 0$). The

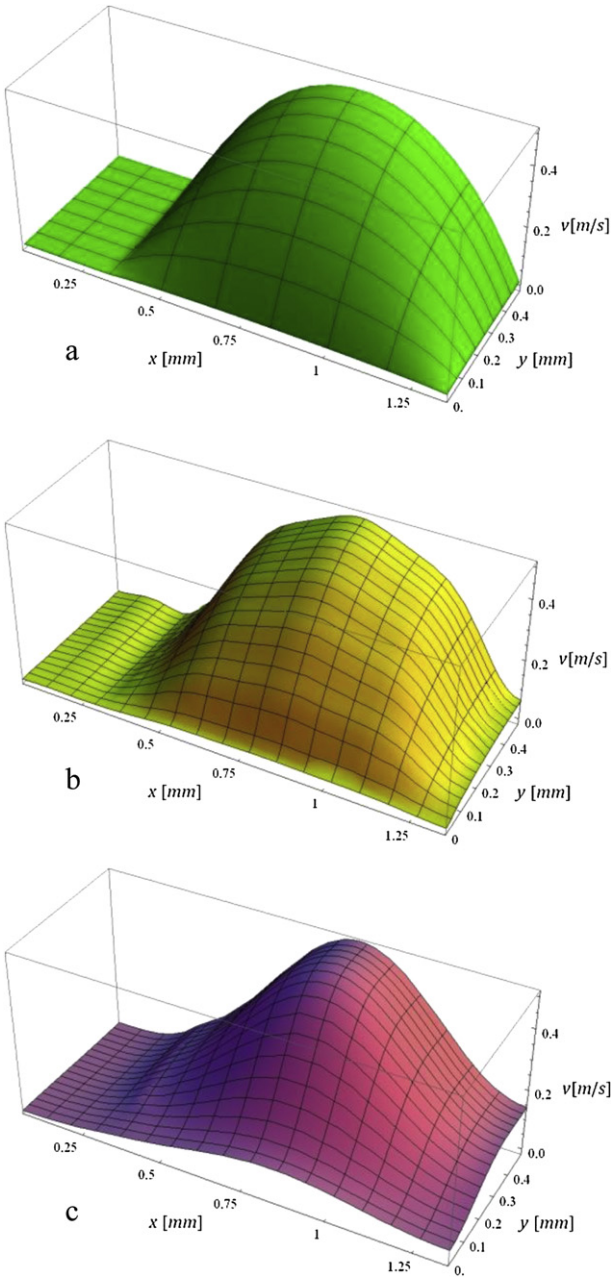

Fig. 7. Plots of velocity profile: (a) CFD, (b) HAN with 10 × 10 harmonics, (c) HAN with 3 × 5 harmonics.

latter is due to strong electroosmotic pull and relatively small concentration gradient across the membrane near the inlets. As the gradient increases, causing increased back diffusion, the relative humidity in anode levels off. Due to only small differences between the CFD and HAN the two are hardly distinguished from one another in this comparative plot.

The pressure drop from the inlets to the outlets is due to the simple geometry and relatively low velocities only few Pascals and thus the total molar concentration c_0 of the gas is practically constant in the whole fuel cell. This means that the concentration of the other component which is either oxygen on cathode side or hydrogen on anode side, is, according to Equation (4), complementary to the concentration of water vapour. The information on the concentration of reactant, shown in Fig. 10, is thus in case of HAN obtained by taking the complement of the concentration of water vapour.

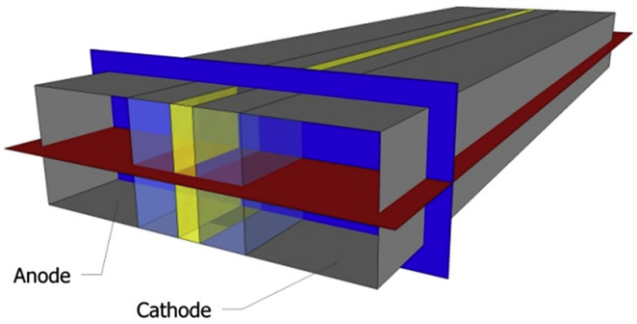

Fig. 8. Section planes in which concentration distributions are plotted. Red plane is at $y = 0.5$ mm and concentration profiles in this plane are presented in Figs. 9 and 10. Blue plane is at $z = 14$ mm and concentration profile of water vapour in this plane is presented in Fig. 11. (For interpretation of the references to colour in this figure legend, the reader is referred to the web version of this article.)

Fig. 10 shows the distribution of molar fraction of reactant: oxygen on the right side ($x > 0$) and hydrogen on the left ($x < 0$). It is discernible from the picture that although the hydrogen is being consumed on its' way from the inlet to the outlet its concentration in fact rises along the way owing to the strong drainage of water from the anode. Again Fig. 10 shows a good agreement between HAN and CFD.

In Fig. 11 that shows a comparative plot of distribution of relative humidity on the cross sectional cut the distribution of relative humidity in the anode can be seen on the left side and the one for cathode on the right side. Also evident is the brake in the slope at the GDL/channel boundary owing to the discontinuity of properties of media. Here the slight differences between the CFD and HAN are more visible. There are two major contributors to the difference

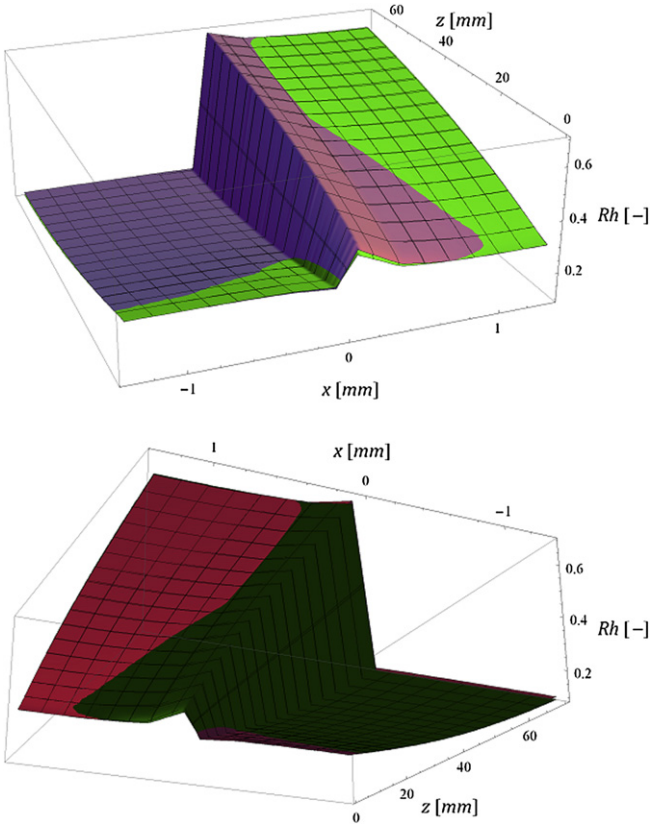

Fig. 9. Plot of distribution of relative humidity over the symmetry plane at $y = 0.5$ mm i.e. the red section plane in Fig. 8. Both plots represent the same concentration profile viewed from two different perspectives. Green and purple surface represent CFD and HAN results respectively. (For interpretation of the references to colour in this figure legend, the reader is referred to the web version of this article.)

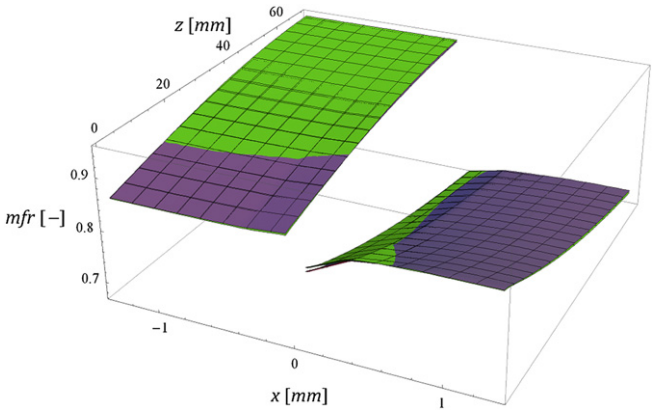

Fig. 10. Plot of distribution of molar fraction of reactant over the symmetry plane at $y = 0.5$ mm i.e. the red section plane in Fig. 8. Green and purple surface represent CFD and HAN results respectively. (For interpretation of the references to colour in this figure legend, the reader is referred to the web version of this article.)

between the concentration profiles calculated by CFD and HAN: The first one is the difference in membrane water transport model. HAN calculates the concentration gradient based only on the values of water content at the boundaries with the two gas elements, whereas CFD divides the thickness of the membrane in 12 discrete sections. Additionally CFD also takes into account a correction of the membrane water diffusion constant as a linear function of membrane water content [21] whereas HAN assumes a single value for this diffusion constant over the whole membrane. HAN's membrane model consequentially either slightly over- or underestimates the rate of water transport over the membrane (assumption XV). The second contributor is the assumption of zero velocity in GDL itself. In addition to the zero value of the z component of velocity this assumption of course means also zero value of the x component of velocity. However, in cases where both components of the gas (i.e. water vapour and reactant) migrate towards the membrane (as for example around the anode inlet) the net gas velocity does have a small component in x coordinate pointing towards the membrane. This although small but nevertheless nonzero value is of course neglected by this assumption of zero velocity in GDL. Both these two contributors are responsible for the slightly different water concentrations and concentration gradients at the membrane/GDL boundary as seen in Fig. 11.

Fig. 11 also reveals that there is hardly any variation of concentration along y coordinate which is due to the very simple geometry of the modelled fuel cell. However some variation is present and it can be extracted by subtracting from the concentration distribution its average along y coordinate. In terms of relative humidity this is:

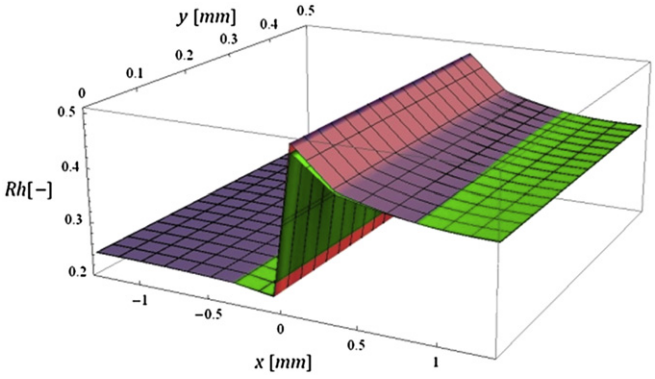

Fig. 11. Plot of distribution of relative humidity over the cross section at $z = 14$ mm i.e. the blue section plane in Fig. 8. Green and purple surface represent CFD and HAN results respectively. (For interpretation of the references to colour in this figure legend, the reader is referred to the web version of this article.)

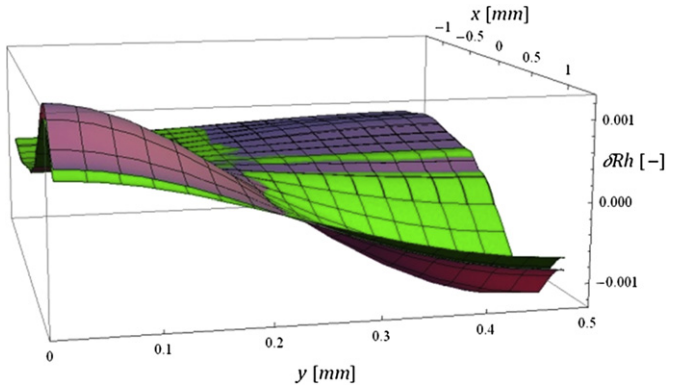

Fig. 12. Plot of δRh i.e. the variation of relative humidity from the average along y coordinate. Green and purple surface represent CFD and HAN results respectively. (For interpretation of the references to colour in this figure legend, the reader is referred to the web version of this article.)

$$\overline{\mathrm{Rh}}(x) = \frac{1}{w}\int_0^w \mathrm{Rh}(x,y)\mathrm{d}y \tag{27}$$

$$\delta\mathrm{Rh}(x,y) = \mathrm{Rh}(x,y) - \overline{\mathrm{Rh}}(x)$$

Fig. 12 reveals that the variation of concentration along y coordinate as calculated by HAN model is very similar to the one calculated by CFD. This variation of concentration is well below overall agreement between the CFD and HAN and is thus practically irrelevant when calibrating and validating HAN on this simple fuel cell. However, the surprisingly close agreement between the two models shows how well the analytical approach of HAN captures the species transport phenomena also along y coordinate.

When HAN model with the higher number of harmonics is used the comparative plots in Figs. 9–12 stay practically identical. The higher accuracy of HAN model with higher number of harmonics does not bring a better agreement with CFD since the major contributor to the differences between HAN and CFD are the difference in the membrane model and the assumption of zero value of the x component of velocity in GDL which do not change with higher number of harmonics. This also shows that the small nonzero values of the z component of velocity in GDL inherent to HAN do not have a significant influence on results. Namely HAN with the higher number of harmonics features smaller deviations from the assumed zero value of the z component of velocity yet it does not produce a better agreement with CFD results.

5.2. Computational times

Since the HAN model calculates only the species transport whereas the CFD simulation calculates also all of the electrochemistry, the computational times of the two are not directly comparable. To obtain an estimate on what portion of computational time the CFD simulation spends just on species transport calculations a dummy CFD simulation was performed having the fuel cell features (i.e. electrochemistry) switched off. The time it takes this dummy CFD simulation to do the same number of iterations as FC CFD simulation serves as a rough estimate of the portion of time required for species transport calculations in the fuel cell simulations The computational times are summarized in Table 1.

Due to the nature of CFD calculation principle the CFD simulation requires from few hundred to few thousand iterations to converge to the solution, HAN on the other hand only needs a few iterations to come up with the correct outlet pressure. In the case of this straight fuel cell and the gas velocities used the pressure drop was only few Pascals and thus very accurate results could have been obtained in a single iteration. Additionally it has to be noted that HAN model evaluated in this paper is programmed in Mathematica programming language that is not best suited for numerical computation thus even shorter computational times are expected when programmed in a more suitable programming language such as C or Fortran. The small difference between the computational times of HAN with 15 harmonics and HAN with a single harmonic, which is in fact a purely 1D model, confirms that the analytic part of HAN does not greatly increase the computational load when a moderate number of harmonics is used. However, on the other hand, HAN with very high number of harmonics also requires much longer computational times although it does not necessarily provide more accurate results as has been show in the previous section.

Table 1
Calculation time (All models were run on same computer).

Model	No. of iterations	CPU cores used	CPU time [s]	Total time [s]
CFD	5000	4	9640	2430
CFD (FC off)	5000	1	6070	6120
HAN (15 hrm)	1	1	0.33	0.33
HAN (100 hrm)	1	1	1.62	1.62
HAN (1 hrm)	1	1	0.22	0.22

At this point it is worth commenting on the choice of solving diffusion equation on a single domain comprising both the channel and the GDL region (outlined in Subsection 3.1.1): The alternative of splitting it onto two domains, each for each region, introduces additional coupling conditions at the GDL/channel interface which increase computational load. The single domain approach presented in this paper leads to only four algebraic equations, given in Section A.3 of Appendix A, for each slice which is the core of the model's computational efficiency. However the ability of defining harmonics on a single domain is inherent to the simple geometry of the modelled fuel cell. For modelling fuel cells with less simple geometry the approach with multiple simple domains, as outlined at the end of Subsection 3.3, could be the preferred approach, since devising harmonics on a single, complex and generally non-rectangular domain could be much more difficult.

6. Conclusion

The paper presented Hybrid Analytic-Numerical (HAN) approach to species transport modelling in a simple fuel cell. HAN is an innovative approach to fuel cell modelling that takes advantage of the 1D numerical treatment of gas flow and the computational efficiency of the analytic 2D solution for the species concentration profile in the plane perpendicular to the gas flow. The overall 3D species concentration distribution calculated by this approach shows a remarkably good agreement with the simulation results obtained by a validated fuel cell purpose full 3D CFD commercial software programme. Additionally it has to be noted that this agreement is achieved already with a very moderate number of harmonics taken into account. The analysis of computational times showed that HAN with this number of harmonics is indeed not considerably slower than 1D models. This computational efficiency together with its very adequately calculated 3D concentration distribution make HAN a very promising model for fuel cell simulations that require short computational times such as in system level applications. The principles of HAN model have been demonstrated on a simple straight channel fuel cell, however, the HAN model can be further extended to model also fuel cells with more complex geometries by efficiently splitting the diffusion

system onto multiple definition domains for eigen functions and by extending the principle of using sink and source terms for treating the convective species transport also in various directions in GDL together with a more complex routine for calculating gas flow in channels and GDL.

Appendix A. Mathematical derivation

The steady state solution for the complete fuel cell is made of consecutive steady state solutions for each slice. In this section a derivation of the solution for a slice is presented. First a partial solution for the gas element shall be constructed than a partial solution for the membrane element and finally the complete solution shall be obtained by coupling the two adjacent cathode and anode gas elements via the membrane element. The derivation makes the assumptions described in the Section 2.

A.1. Gas element

This subsection deals with the partial solution for gas element that is schematically depicted in Fig. 3. First the diffusion problem shall be defined in this coordinate system, following with the construction of the two types of eigen functions: eigen functions dealing with convective (source and sink) terms and eigen functions dealing with diffusion from membrane. In the end the linear combinations of eigen functions shall be presented in vector notation and the whole diffusion problem translated into an algebraic form.

A.1.1. Diffusion differential equation

Gas element is coupled to three neighbour elements: It is coupled to the neighbour gas element upstream and to the one downstream via the source and sink term (Equations (9) and (10)) and to the membrane element via the boundary condition (12). Each of these three couplings has its own contribution to the influx of species into the gas element. Thus the concentration distribution can be split into three independent contributions reflecting the influx contribution of each of the couplings:

$$c(x,y) = c^{\mathrm{src}}(x,y) + c^{\mathrm{dff}}(x,y) - c^{\mathrm{snk}}(x,y), \tag{A1}$$

where c^{src} is the contribution to c solely from the source term, $-c^{\mathrm{snk}}$ the contribution solely from the sink term and c^{dff} the contribution solely from the diffusion from the membrane. In the following derivation the construction of these contributions shall be such that each contribution does not interfere with the influx coupling conditions of the other two. By doing this each contribution is fully defined solely by its corresponding influx coupling condition. Thus the overall concentration distribution is a sum of the three contributions. Their interdependence is limited to only two conditions: Their sum must be a stationary solution (i.e. time independent) and the value of their sum at the interface with membrane has to couple appropriately to the membrane water content at that interface.

Due to linearity of the diffusion equation the Equation (8) can simply be split into:

$$\frac{\partial c^{\mathrm{src}}(x,y)}{\partial t} = D\nabla^2 c^{\mathrm{src}}(x,y) + s^{\mathrm{src}}(x,y), \tag{A2}$$

$$\frac{\partial c^{\mathrm{snk}}(x,y)}{\partial t} = D\nabla^2 c^{\mathrm{snk}}(x,y) + s^{\mathrm{snk}}(x,y), \tag{A3}$$

$$\frac{\partial c^{\mathrm{dff}}(x,y)}{\partial t} = D\nabla^2 c^{\mathrm{dff}}(x,y), \tag{A4}$$

The Equations (A2) and (A3) already reveal that c^{src} and c^{snk} do not interfere with each other's influx coupling condition since c^{src} assumes no outflow and thus doesn't add anything to the s^{snk} term and vice-versa is true for the c^{snk}. The three contributions also satisfy the following boundary conditions:

$$\left.\frac{\partial c^{\mathrm{dff}}(x,y)}{\partial n}\right|_{\mathrm{wall}} = 0; \quad \left.\frac{\partial c^{\mathrm{dff}}(x,y)}{\partial x}\right|_{x=h} = \frac{j(y)}{\kappa D_{\mathrm{GDL}}}, \tag{A5}$$

$$\left.\frac{\partial c^{\mathrm{src}}(x,y)}{\partial n}\right|_{wall} = \left.\frac{\partial c^{\mathrm{snk}}(x,y)}{\partial n}\right|_{\mathrm{wall}} = \left.\frac{\partial c^{\mathrm{src}}(x,y)}{\partial x}\right|_{x=h} = \left.\frac{\partial c^{\mathrm{snk}}(x,y)}{\partial x}\right|_{x=h} = 0, \tag{A6}$$

$$D_{chnl}\left.\frac{\partial c^{\mathrm{dff,src,snk}}(x,y)}{\partial x}\right|_{x=d^-} = \kappa D_{\mathrm{GDL}}\left.\frac{\partial c^{\mathrm{dff,src,snk}}(x,y)}{\partial x}\right|_{x=d^+}. \tag{A7}$$

In this way all of the water flux from membrane to the gas-flow element, schematically represented by the green arrow in Fig. 3, is accounted for by the c^{dff} concentration distribution contribution and both convective contributions i.e. c^{src}, c^{snk} assume no water exchange with the membrane and thus have zero normal gradient at the membrane-GDL interface. This additionally means that c^{src} and c^{snk} do not interfere with the influx coupling conditions that give rise to c^{dff}. The requirement that c^{dff} also does not interfere with the influx coupling conditions of the other two shall be fulfilled after constructing c^{dff} in Subsection A.1.2.2.

It should be noted that expressions in Equations (A2), (A3) and (A4) by themselves do not equal zero. This is only the case of their sum which is Equation (8).

Combining Equations (10), (11) and (A1) gives

$$s^{\mathrm{snk}}(x,y) = \frac{1}{l}\tilde{v}u(x,y)\left(c^{\mathrm{src}}(x,y) + c^{\mathrm{dff}}(x,y) - c^{\mathrm{snk}}(x,y)\right). \tag{A8}$$

Using Equation (A8) in Equation (8) gives:

$$D\nabla^2\left(c^{\mathrm{src}} + c^{\mathrm{dff}} - c^{\mathrm{snk}}\right) + s^{\mathrm{src}} - \frac{1}{l}v\left(c^{\mathrm{src}} + c^{\mathrm{dff}} - c^{\mathrm{snk}}\right) = 0. \tag{A9}$$

Here the notation with reference to (x, y) dependence has been left out for brevity.

The presented way of splitting the overall concentration into the three types of contributions: c^{src}, c^{snk} and c^{dff} can be applied also in cases of more complex fuel cell geometries. Following the outline at the end of Subsection 3.3 the diffusion problem can be split onto multiple domains where each domain always couples to other domains only via the three aforementioned types of influx coupling conditions that give rise to these three types of contributions. Generally, each coupling interface can assume any of the three types of influx coupling conditions.

A.1.2. Eigen functions

A general distribution of concentration of a contribution that satisfies given boundary conditions can be represented by a linear combination of the eigen functions of the $D\nabla^2$ operator (this operator applies to both channel domain and the GDL domain with the D taking on value of D_{chnl} in channel and D_{GDL} in GDL).

A.1.2.1. Eigen functions for convective terms. The two convective contributions c^{src} and c^{snk} are governed by Equations (A2) and (A3) and satisfy boundary conditions (A6). Let $\Psi_{m,n}(x, y)$ be an eigen function of the $D\nabla^2$ operator satisfying the same boundary conditions (A6), than a general convective concentration distribution satisfying these boundary conditions $c^{\mathrm{cnv}}(x, y)$ can be written as:

$$c^{cnv}(x,y) = \sum_{m,n} c^{cnv}_{m,n}\Psi_{m,n}(x,y), \tag{A10}$$

where $c^{cnv}_{m,n}$ are the coefficients. Here the superscript cnv stands for either src or snk. Similarly as any function defined on $h \times w$ definition region of gas element can be expressed as a linear combination of $\Psi_{m,n}(x, y)$ eigen functions so can be $s^{cnv}(x, y)$:

$$s^{cnv}(x,y) = \sum_{m,n} s^{cnv}_{m,n}\Psi_{m,n}(x,y), \tag{A11}$$

where $s^{cnv}_{m,n}$ are the coefficients. With $\lambda_{m,n}$ as the eigen value of $\Psi_{m,n}(x, y)$ the Equations (A2) (or (A3)) and (A11) give:

$$\begin{aligned}\frac{\partial c^{cnv}(x,y)}{\partial t} &= D\nabla^2\sum_{m,n} c^{cnv}_{m,n}\Psi_{m,n}(x,y) + \sum_{m,n} s^{cnv}_{m,n}\Psi_{m,n}(x,y)\\ &= \sum_{m,n}\lambda_{m,n}c^{cnv}_{m,n}\Psi_{m,n}(x,y) + \sum_{m,n} s^{cnv}_{m,n}\Psi_{m,n}(x,y).\end{aligned} \tag{A12}$$

A steady state solution $\partial c^{cnv}/\partial t = 0$ is obtained by setting:

$$c^{cnv}_{m,n} = -\frac{s^{cnv}_{m,n}}{\lambda_{m,n}} \tag{A13}$$

and thus

$$c^{cnv}(x,y) = -\sum_{m,n}\frac{s^{cnv}_{m,n}}{\lambda_{m,n}}\Psi_{m,n}(x,y). \tag{A14}$$

However, this only applies to eigen functions with nonzero eigen values ($\lambda_{m,n} \neq 0$). When one of the components of $s^{cnv}(x, y)$ is also the $\Psi_{zero}(x, y)$ eigen function with eigen value $\lambda_{zero} = 0$ than the corresponding coefficient c^{cnv}_{zero} in $c^{cnv}(x, y)$ needs special treatment. This will be presented after first constructing the complete family of $\Psi_{m,n}$ eigen functions.

These Ψ eigen functions, constructed on the definition region comprising both the GDL and the channel domain i.e. on the $h \times w$ rectangle, are as follows:

$$\Psi_{m,n}(x,y) = \cos\left(\frac{m\pi}{w}y\right)\mathrm{TRIG}_{m,n}(x) \tag{A15}$$

$$\mathrm{TRIG}_{m,n}(x) = \begin{cases}\cos(k_{1,m,n}(h-x)) & x\in \mathrm{GDL}\\ \gamma_{m,n}\cos(k_{2,m,n}x) & x\in \mathrm{channel}\end{cases} \tag{A16}$$

$\Psi_{m,n}$ are in fact cos ($k_x x$)cos ($k_y y$) harmonics constructed on the definition region comprising two domains with different material properties. For calculating $k_{1,m,n}$, $k_{2,m,n}$ and $\gamma_{m,n}$ see Appendix C. The zero gradient normal to the boundary required by (A6) is reflected in the choice of cos that has zero normal derivative at all the boundaries.

The Ψ_{zero} eigen function is identified as $\Psi_{0,0}(x, y) = 1$, which indeed has the eigen value of zero. The source (or sink) term $s^{cnv}(x, y)$ specifies convective flow of water vapour into (or out of) the gas element where all but one of its $s^{cnv}_{m,n}\Psi_{m,n}(x, y)$ components have zero net inflow (or outflow) contribution. The exception is exactly the $s^{cnv}_{0,0}\Psi_{0,0}(x, y)$ component that defines how much water overall is convectively entering (exiting) the element. With constant net inflow (outflow) the c^{cnv} contribution must linearly rise (fall) with time which is revealed by the Equation (A2) (or (A3)) reduced onto the $\Psi_{0,0}(x,y)$ component:

$$\begin{aligned}&\frac{\partial\left(c^{cnv}_{0,0}\Psi_{0,0}(x,y)\right)}{\partial t} = D\nabla^2\left(c^{cnv}_{0,0}\Psi_{0,0}(x,y)\right) + s^{cnv}_{0,0}\Psi_{0,0}(x,y)\Rightarrow\\ &\frac{\partial c^{cnv}_{0,0}}{\partial t}\Psi_{0,0}(x,y) = 0 + s^{cnv}_{0,0}\Psi_{0,0}(x,y)\Rightarrow\frac{\partial c^{cnv}_{0,0}}{\partial t} = s^{cnv}_{0,0}.\end{aligned} \tag{A17}$$

Equation (A17) is solved by a linear function of time with an ansatz $c^{cnv}_{0,0} = c^{cnv}_t t + c^{cnv}_{intg}$ that has a simple solution for c^{cnv}_t:

$$c^{cnv}_t = s^{cnv}_{0,0}, \tag{A18}$$

The remaining integration constant c^{cnv}_{intg} is to be defined later by the final solution of coupling partial solutions. Altogether the $c^{cnv}(x, y)$ can be expressed as:

$$\begin{aligned}c^{cnv}(x,y) &= \sum_{\substack{m,n\\ m\wedge n\neq 0}} c^{cnv}_{m,n}\Psi_{m,n}(x,y) + \left(c^{cnv}_t t + c^{cnv}_{intg}\right)\Psi_{0,0}(x,y)\\ &= -\sum_{\substack{m,n\\ m\wedge n\neq 0}}\frac{s^{cnv}_{m,n}}{\lambda_{m,n}}\Psi_{m,n}(x,y) + s^{cnv}_{0,0}t + c^{cnv}_{intg},\end{aligned} \tag{A19}$$

(the latter expression acknowledges that $\Psi_{0,0}(x, y) = 1$). The time dependence in this solution may seem to work against the goal of finding a steady state solution, but it has to be noted that a steady state solution of the whole concentration distribution is sought which leads to the requirement that the time dependant terms of all the contributions must cancel each other out. This condition shall be concretely defined after constructing the other type of eigen functions.

A.1.2.2. Eigen functions for diffusive flow from membrane. The c^{dff} contribution is governed by Equation (A4) and satisfies boundary conditions (A5). The molar flux of water from membrane to gas element $j(y)$ found in this boundary condition expressed as linear combination of cos harmonics reads:

$$j(y) = \sum_{m=0}^{\infty} j_m\cos\left(\frac{m\pi}{w}y\right) \tag{A20}$$

where j_m are the corresponding coefficients. Let $\Phi_m(x,y)$, be an eigen function satisfying the boundary condition

$$\left.\frac{\partial\Phi_m(x,y)}{\partial n}\right|_{wall} = 0, \quad \kappa D_{GDL}\left.\frac{\partial\Phi_m(x,y)}{\partial x}\right|_{x=h} = \cos\left(\frac{m\pi}{w}y\right), \tag{A21}$$

than a linear combination of eigen functions

$$c^{dff}(x,y) = \sum_{m=0}^{\infty} c^{dff}_m\Phi_m(x,y), \tag{A22}$$

with

$$c^{dff}_m = j_m \tag{A23}$$

satisfies the boundary condition

$$\kappa D_{GDL}\left.\frac{\partial c^{dff}(x,y)}{\partial x}\right|_{x=L} = \sum_{m=0}^{\infty} j_m\cos\left(\frac{m\pi}{w}y\right) = j(y) \tag{A24}$$

Let, for $m \neq 0$, the Φ_m satisfy also the stationary diffusion equation:

$$\frac{\partial \Phi_m}{\partial t} = D\nabla^2 \Phi_m = 0. \tag{A25}$$

(The latter implies that for $m \neq 0$ all Φ_m eigen functions have zero eigen value. Here again the case of $m = 0$ is special and will be dealt with separately.) The family of eigen functions $\Phi_m(x,y), m \neq 0$ satisfying conditions (A21) and (A25) is constructed in the following way:

$$\Phi_m(x,y) = \cos\left(\frac{m\pi}{w}y\right)\mathrm{HYPTRG}_m(x), \tag{A26}$$

$$\mathrm{HYPTRG}_m(x) = \begin{cases} a_m e^{\frac{m\pi}{w}(h-x)} + b_m e^{-\frac{m\pi}{w}(h-x)} & x \in \mathrm{GDL} \\ \alpha_m \cosh\left(\frac{m\pi}{w}x\right) & x \in \mathrm{channel} \end{cases} \tag{A27}$$

with a_m, α_m, and b_m defined in Appendix D. The choice of cos and cosh functions also accounts for the boundary condition at other three remaining walls: $(\partial \Phi_m(x,y)/\partial n)|_{\mathrm{wall}} = 0$. Similar to $\Psi_{m,n}$ the Φ_m eigen functions are cos (ky)cosh (kx) harmonics with eigen values of zero $(D\nabla^2 \Phi_m = 0, m \neq 0)$ constructed on a definition region comprising two domains with different material properties. Here it can be seen that the so constructed eigen functions of c^{dff} do not interfere with the influx coupling conditions of c^{cnv} since, due to their Laplace being zero, adding them to c^{src} or c^{snk} has no influence on Equation (A2) or (A3), again the exception being the $m = 0$ case.

In the special case of $m = 0$, i.e. the constant term in expression (A20) for the molar flux of water, there can be no nonzero steady state solution. The rationale is similar to the previous case of $\Psi_{0,0}$: In $j(y)$ all its' $\cos((m\pi/w)y)$ components, with $m \neq 0$, have zero net contribution to the flow of water from membrane into the gas element (the average of cos is zero). On the other hand the $m = 0$ component in $j(y)$ is 1 and it is thus the only component that accounts for the net water inflow. Again, with constant net inflow the c^{dff} contribution must linearly rise with time. The boundary conditions (A21) for $\Phi_0(x, y)$ read:

$$\left.\frac{\partial \Phi_0(x,y)}{\partial n}\right|_{\mathrm{wall}} = 0, \kappa D_{\mathrm{GDL}} \left.\frac{\partial \Phi_0(x,y)}{\partial x}\right|_{x=h} = 1, \tag{A28}$$

where 1 on the right-hand-side means there is net inflow. Thus, the Equation (A25) does not hold for $m = 0$ but instead:

$$\frac{\partial \Phi_0}{\partial t} = D\nabla^2 \Phi_0 = \omega, \tag{A29}$$

where ω is a geometrical factor to be defined after constructing Φ_0. The solution for Φ_0 satisfying conditions (A28) and (A29) is constructed as follows:

$$\Phi_0 = SQR(x,y) + \omega t + \xi, \tag{A30}$$

where ξ is an integration constant and SQR(x, y) is such that $D\nabla^2 \mathrm{SQR}(x, y) = \omega$ and such that it takes care of condition (A28):

$$\mathrm{SQR}(x,y) = \begin{cases} \frac{\omega}{2D_{\mathrm{GDL}}}(h-x)^2 - \frac{1}{\kappa D_{\mathrm{GDL}}}(h-x) & x \in \mathrm{GDL} \\ \frac{\omega}{2D_{\mathrm{chnl}}}x^2 - \beta_0 & x \in \mathrm{channel} \end{cases} \tag{A31}$$

where continuity of SQR(x, y) requires that

$$\mathrm{SQR}\left(x = d^+, y\right) = \mathrm{SQR}\left(x = d^-, y\right) \Rightarrow$$
$$\beta_0 = \frac{\omega d^2}{2D_{\mathrm{chnl}}} - \frac{\omega(h-d)^2}{2D_{\mathrm{GDL}}} + \frac{(h-d)}{\kappa D_{\mathrm{GDL}}} \tag{A32}$$

ω is defined by the requirements for continuity of flux between GDL and channel:

$$\begin{aligned} j_{\mathrm{GDL}}|_{x=d} &= j_{\mathrm{chnl}}|_{x=d} \Rightarrow \kappa D_{\mathrm{GDL}} \left.\frac{\partial \mathrm{SQR}(x,y)}{\partial x}\right|_{x=d^+} \\ &= D_{\mathrm{chnl}} \left.\frac{\partial \mathrm{SQR}(x,y)}{\partial x}\right|_{x=d^-} \Rightarrow -\omega\kappa(h-d) + 1 = \omega d \\ &\Rightarrow \omega = d + \kappa(h-d) \end{aligned} \tag{A33}$$

Summing all up the Equation (A22) in more detail reads:

$$\begin{aligned} c^{\mathrm{dff}}(x,y) &= \sum_{m=0}^{\infty} c_m^{\mathrm{dff}} \Phi_m(x,y) \\ &= \sum_{m=1}^{\infty} c_m^{\mathrm{dff}} \Phi_m(x,y) + c_0^{\mathrm{dff}} SQR(x,y) + c_t^{\mathrm{dff}} t + c_{\mathrm{intg}}^{\mathrm{dff}} \end{aligned} \tag{A34}$$

where

$$c_t^{\mathrm{dff}} = \omega c_0^{\mathrm{dff}}, \tag{A35}$$

and the integration constant $c_{\mathrm{intg}}^{\mathrm{dff}} = c_0^{\mathrm{dff}}\xi$. This integration constant is to be defined later by the final solution of coupling partial solutions.

A.1.2.3. Additional conditions for sum of all contributions. Each of the three contributions contains two terms (the integration constant and the time dependant term) that must satisfy additional conditions when all three contributions are put together. All three contributions $c^{\mathrm{src}}(x, y)$, $c^{\mathrm{snk}}(x, y)$ and $c^{\mathrm{dff}}(x, y)$ bring about integration constants that amount to:

$$c_{\mathrm{intg}} = c_{\mathrm{intg}}^{\mathrm{src}} - c_{\mathrm{intg}}^{\mathrm{snk}} + c_{\mathrm{intg}}^{\mathrm{dff}}. \tag{A36}$$

When coupling the partial solution of a gas element with the other two in a slice only the overall c_{intg} shall be defined allowing for an arbitrary distribution of its value among $c_{\mathrm{intg}}^{\mathrm{src}}$, $c_{\mathrm{intg}}^{\mathrm{snk}}$ and $c_{\mathrm{intg}}^{\mathrm{dff}}$. In the process of obtaining the partial solution for a gas element the unknown of sink term shall be solved for by treating the source term and diffusion flow from membrane as parameters (as presented in the next A.1.3 section), therefore the following choice is most practical:

$$c_{\mathrm{intg}}^{\mathrm{src}} = c_{\mathrm{intg}}^{\mathrm{dff}} = 0, \quad c_{\mathrm{intg}}^{\mathrm{snk}} = -c_{\mathrm{intg}}. \tag{A37}$$

By doing this, the three contributions expressed as linear combinations from Equations (A19) and (A34) become:

$$c^{\mathrm{src}}(x,y) = \sum_{\substack{m,n \\ m \wedge n \neq 0}} c_{m,n}^{\mathrm{src}} \Psi_{m,n}(x,y) + c_t^{\mathrm{src}} t \tag{A38}$$

$$c^{\mathrm{snk}}(x,y) = \sum_{\substack{m,n \\ m \wedge n \neq 0}} c_{m,n}^{\mathrm{snk}} \Psi_{m,n}(x,y) + c_t^{\mathrm{snk}} t - c_{\mathrm{intg}} \tag{A39}$$

$$c^{\mathrm{dff}}(x,y) = \sum_{m=1}^{\infty} c_m^{\mathrm{dff}} \Phi_m(x,y) + c_0^{\mathrm{dff}} \mathrm{SQR}(x,y) + c_t^{\mathrm{dff}} t, \tag{A40}$$

The so defined three contributions may be negative in some parts of the definition region. Negative concentration is not physical, but here only the expression for total concentration c needs to be physically sound, the three partial contributions by themselves

only need to satisfy their corresponding diffusion equations and boundary conditions.

The diffusion Equation (8) is a steady state equation and thus its solution cannot contain any time dependence. This means that the three contributions that do contain time dependence by themselves must add together in such a way that this time dependence vanishes. In order to satisfy the steady state condition for the overall solution of concentration distribution in a gas element the time dependant terms in each of the three contributions must cancel each other out

$$\frac{\partial c(x,y)}{\partial t} = \frac{\partial\left(c^{\mathrm{src}}(x,y) - c^{\mathrm{snk}}(x,y) + c^{\mathrm{dff}}(x,y)\right)}{\partial t} = \frac{\partial\left(c_t^{\mathrm{src}} t - c_t^{\mathrm{snk}} t + c_t^{\mathrm{dff}} t\right)}{\partial t} = 0, \tag{A41}$$

leading to the following condition:

$$c_t^{\mathrm{src}} - c_t^{\mathrm{snk}} + c_t^{\mathrm{dff}} = 0. \tag{A42}$$

In the following algebraic manipulation (section A.1.3) satisfying this condition (A42) is crucial for obtaining physically meaningful steady state solution.

A.1.3. Vector notation and algebraic manipulation

In this subsection the equations from previous section containing sums over the families of harmonics will be written in a convenient compact vector form. Having established the vector notation the partial solution for a gas element shall be obtained by algebraic manipulation. This partial solution shall be obtained by treating the source term and diffusion flow from membrane as parameters and have the algebraic manipulation solve for the unknowns of the sink term and concentration distribution.

For the purpose of computational feasibility the number of harmonics taken into account in sums such as in expressions (A38), (A39) and (A40) should be limited. Greater number of harmonics improves accuracy but lengthens computational times. Let $M+1$ be the maximal number of harmonic-indices in y coordinate and $N+1$ the maximal number of harmonic-indices in x coordinate (i.e. index m running from 0 to M and index n from 0 to N). This means total number of $\Psi_{m,n}$ harmonics is $(M+1)(N+1)$ and total number of Φ_m harmonics is $(M+1)$. Having a finite number of $\Psi_{m,n}$ eigen functions allows for a simple indexing with only one index. By defining:

$$\theta = n(M+1) + m, \tag{A43}$$

the double index m, n is uniquely replaced by single index θ that runs from 0 to $\Theta = NM + N + M$ (altogether $(M+1)(N+1)$ indices). Thus: $\Psi_{0,0} \to \Psi_0, \Psi_{0,1} \to \Psi_1, \ldots, \Psi_{m,n} \to \Psi_\theta, \ldots, \Psi_{M,N} \to \Psi_\Theta$. This θ indexing will come in handy for gathering all eigen functions $\Psi_{m,n} = \Psi_\theta$ and other double index elements into vectors. Conversely, m and n are extracted from θ by modulo division mod and integer division $\div$:

$$m = m(\theta) = \theta \bmod (M+1), \quad n = n(\theta) = \theta \div (M+1). \tag{A44}$$

Starting with sum (A38) and (A39) and taking into account the limited number of terms in sums the upper sums are written in following vector form:

$$c^{\mathrm{src}}(x,y) \approx \sum_{n=0}^{N} \sum_{\substack{m=0 \\ m \wedge n \neq 0}}^{M} c_{m,n}^{\mathrm{src}} \Psi_{m,n}(x,y) + c_t^{\mathrm{src}} t = \sum_{\theta=1}^{\Theta} c_\theta^{\mathrm{src}} \Psi_\theta(x,y) + c_t^{\mathrm{src}} t = \vec{c}^{\,\mathrm{src}} \cdot \vec{\Psi} + c_t^{\mathrm{src}} t \tag{A45}$$

$$c^{\mathrm{snk}}(x,y) \approx \sum_{n=0}^{N} \sum_{\substack{m=0 \\ m \wedge n \neq 0}}^{M} c_{m,n}^{\mathrm{snk}} \Psi_{m,n}(x,y) - c_{\mathrm{intg}} + c_t^{\mathrm{snk}} t = \sum_{\theta=1}^{\Theta} c_\theta^{\mathrm{snk}} \Psi_\theta(x,y) + c_t^{\mathrm{snk}} t - c_{\mathrm{intg}} = \vec{c}^{\,\mathrm{snk}} \cdot \vec{\Psi} + c_t^{\mathrm{snk}} t \tag{A46}$$

where the family of $\Psi_\theta(x,y)$ eigen functions forms vector $\vec{\Psi}$ and the coefficients are gathered in vector $\vec{c}^{\,\mathrm{cnv}}$ as follows:

$$\vec{\Psi} = (\Psi_0(x,y)(=1), \Psi_1(x,y), \Psi_2(x,y), \ldots, \Psi_\Theta(x,y))^T, \tag{A47}$$

$$\vec{c}^{\,\mathrm{src}} = (0, c_1^{\mathrm{src}}, c_2^{\mathrm{src}}, \ldots, c_\Theta^{\mathrm{src}})^T, \tag{A48}$$

$$\vec{c}^{\,\mathrm{snk}} = \left(-c_{\mathrm{intg}}, c_1^{\mathrm{snk}}, c_2^{\mathrm{snk}}, \ldots, c_\Theta^{\mathrm{snk}}\right)^T. \tag{A49}$$

The first component in $\vec{c}^{\,\mathrm{cnv}}$ reflects the choice (A37) setting the constant term coefficient to $c_{\mathrm{intg}}^{\mathrm{src}} = 0$ and $c_{\mathrm{intg}}^{\mathrm{snk}} = -c_{\mathrm{intg}}$. These vectors have dimension of $(M+1)(N+1)$ and are denoted with $\vec{}$. This is important since, later, vectors of different dimension will be introduced.

Furthermore, $\vec{c}^{\,\mathrm{src}}$ is, together with Equation (A13) i.e. $c_\theta^{\mathrm{cnv}} = -s_\theta^{\mathrm{cnv}}/\lambda_\theta$ and (A18) i.e. $c_t^{\mathrm{cnv}} = s_0^{\mathrm{cnv}}$ expressed as:

$$c^{\mathrm{src}}(x,y) = \vec{c}^{\,\mathrm{src}} \cdot \vec{\Psi} + c_t^{\mathrm{src}} t = \left(\overline{B}\,\vec{s}^{\,\mathrm{src}}\right) \cdot \vec{\Psi}, \tag{A50}$$

where

$$\vec{s}^{\,\mathrm{cnv}} = (s_0^{\mathrm{cnv}}, s_1^{\mathrm{cnv}}, s_2^{\mathrm{cnv}}, \ldots, s_\Theta^{\mathrm{cnv}})^T, \tag{A51}$$

$$\overline{B} = \begin{bmatrix} t & 0 & \cdots & 0 \\ 0 & \frac{-1}{\lambda_1} & \cdots & 0 \\ \vdots & \vdots & \ddots & \vdots \\ 0 & 0 & \cdots & \frac{-1}{\lambda_\Theta} \end{bmatrix}, \tag{A52}$$

$\overline{B}$ has $(t, (-1/\lambda_1), (-1/\lambda_2), \ldots, (-1/\lambda_\theta), \ldots, (-1/\lambda_\Theta))$ on the diagonal. $\overline{B}$ and all following matrices denoted with – are (M+1)(N+1) by $(M+1)(N+1)$ matrices that map from $\vec{}$ vector space to the same $\vec{}$ vector space.

In similar way $\vec{c}^{\,\mathrm{snk}}$ is expressed taking into account that the constant term is the remaining integration constant $c_{\mathrm{intg}}^{\mathrm{snk}} = -c_{\mathrm{intg}}$ that is yet to be defined:

$$c^{\mathrm{snk}}(x,y) = \vec{c}^{\,\mathrm{snk}} \cdot \vec{\Psi} + c_t^{\mathrm{snk}} t = \left(\overline{B}\,\vec{s}^{\,\mathrm{snk}}\right) \cdot \vec{\Psi} - c_{\mathrm{intg}}^{\mathrm{snk}} = \left(\overline{B}\,\vec{s}^{\,\mathrm{snk}}\right) \cdot \vec{\Psi} - c_{\mathrm{intg}}, \tag{A53}$$

Following the same principle, $c^{\mathrm{dff}}(x,y)$ from (A40) together with Equation (A23) i.e. $c_m^{\mathrm{dff}} = j_m$ and (A35) i.e. $c_t^{\mathrm{dff}} = \omega c_0^{\mathrm{dff}}$ is expressed as:

$$\begin{aligned} c^{\mathrm{dff}}(x,y) &= \sum_{m=1}^{M} c_m^{\mathrm{dff}}\Phi_m(x,y) + c_0^{\mathrm{dff}}\mathrm{SQR}(x,y) + c_t^{\mathrm{dff}}t \\ &= \vec{c}^{\,\mathrm{dff}}\cdot\vec{\Phi} + c_t^{\mathrm{dff}}t = \vec{j}\cdot\vec{\Phi} + \omega j_0 t = \vec{j}\cdot\vec{\Phi} + c_t^{\mathrm{dff}}t \end{aligned} \tag{A54}$$

where

$$\vec{\Phi} = (\mathrm{SQR}(x,y), \Phi_1(x,y), \Phi_2(x,y), \ldots, \Phi_M(x,y))^T, \tag{A55}$$

$$\vec{c}^{\,\mathrm{dff}} = \left(c_0^{\mathrm{dff}}, c_1^{\mathrm{dff}}, c_2^{\mathrm{dff}}, \ldots, c_M^{\mathrm{dff}}\right)^T, \tag{A56}$$

$$\vec{j} = (j_0, j_1, j_2, \ldots, j_M)^T, \tag{A57}$$

Here the vectors denoted with $\rightharpoonup$ (not to be confused with $\vec{}$) have dimension of $M+1$. Additionally defining:

$$\vec{\cos} = \left(1, \cos\left(\frac{\pi}{w}y\right), \cos\left(\frac{2\pi}{w}y\right), \cos\left(\frac{3\pi}{w}y\right), \ldots, \cos\left(\frac{M\pi}{w}y\right)\right)^T, \tag{A58}$$

Flux of water into gas element $j(y)$ is expressed as:

$$j(y) = \sum_{m=0}^{M} j_m \cos\left(\frac{m\pi}{w}y\right) = \vec{j}\cdot\vec{\cos} \tag{A59}$$

With this vector notation introduced in Equations (A45), (A46) and (A54) while taking into account the condition (A42) the Equation (A1) can be expressed as:

$$\begin{aligned} c(x,y) &= \vec{c}^{\,\mathrm{src}}\cdot\vec{\Psi} - \vec{c}^{\,\mathrm{snk}}\cdot\vec{\Psi} + \vec{c}^{\,\mathrm{dff}}\cdot\vec{\Phi} + c_t^{\mathrm{src}}t - c_t^{\mathrm{snk}}t + c_t^{\mathrm{dff}}t \\ &= \left(\vec{c}^{\,\mathrm{src}} - \vec{c}^{\,\mathrm{snk}}\right)\cdot\vec{\Psi} + \vec{c}^{\,\mathrm{dff}}\cdot\vec{\Phi} \end{aligned} \tag{A60}$$

Let's introduce a term, denoted by the superscript ss, that gathers the contributions from the source and the sink term and will come in handy later:

$$\begin{aligned} c^{\mathrm{ss}}(x,y) &= c^{\mathrm{src}}(x,y) - c^{\mathrm{snk}}(x,y) \\ &= \left(\vec{c}^{\,\mathrm{src}} - \vec{c}^{\,\mathrm{snk}}\right)\cdot\vec{\Psi} + c_t^{\mathrm{src}}t - c_t^{\mathrm{snk}}t = \vec{c}^{\,\mathrm{ss}}\cdot\vec{\Psi} + c_t^{\mathrm{ss}}t \end{aligned} \tag{A61}$$

with $\vec{c}^{\,\mathrm{src}} - \vec{c}^{\,\mathrm{snk}} = \vec{c}^{\,\mathrm{ss}}$ Equation (A60) thus becomes:

$$c(x,y) = \vec{c}^{\,\mathrm{ss}}\cdot\vec{\Psi} + \vec{c}^{\,\mathrm{dff}}\cdot\vec{\Phi} \tag{A62}$$

Equation (A60) contains $\vec{c}^{\,\mathrm{src}}$ and $\vec{c}^{\,\mathrm{dff}}$ that are already fully defined by the assumed $\vec{c}^{\,\mathrm{src}}$ and $\vec{j}$ and equations (A50) and (A54) and it also contains the unknown $\vec{c}^{\,\mathrm{snk}}$. The following algebraic manipulation will solve for the unknown $\vec{c}^{\,\mathrm{snk}}$. Since $\vec{c}^{\,\mathrm{snk}}$ is defined by (A53), first, expression for $\vec{s}^{\,\mathrm{snk}}$ needs to be found. Combining Equations (10) and (11) and (A62) yields:

$$\vec{s}^{\,\mathrm{snk}}\cdot\vec{\Psi} = s^{\mathrm{snk}}(x,y) = \frac{1}{l}\tilde{\nu}u(x,y)\left(\vec{c}^{\,\mathrm{ss}}\cdot\vec{\Psi} + \vec{c}^{\,\mathrm{dff}}\cdot\vec{\Phi}\right). \tag{A63}$$

Let us express $(1/l)u(x,y)\left(\vec{c}^{\,\mathrm{ss}}\cdot\vec{\Psi}\right)$ and $(1/l)u(x,y)\left(\vec{c}^{\,\mathrm{dff}}\cdot\vec{\Phi}\right)$ as linear combination of Ψ harmonics. A single Ψ_θ harmonic multiplied by the velocity profile is written as:

$$\frac{1}{l}u(x,y)\Psi_\theta(x,y) = \sum_{\mu=0}^{\Theta} V_\mu^\theta \Psi_\mu(x,y) \tag{A64}$$

Having expression for a single harmonic the expression for $(1/l)u(x,y)(\vec{c}^{\,\mathrm{ss}}\cdot\vec{\Psi})$ is:

$$\begin{aligned} \frac{1}{l}u(x,y)\left(\vec{c}^{\,\mathrm{ss}}\cdot\vec{\Psi}\right) &= \frac{1}{l}u(x,y)\sum_{\theta=0}^{\Theta} c_\theta^{\mathrm{ss}}\Psi_\theta(x,y) \\ &= \sum_{\theta=0}^{\Theta}\left(c_\theta^{\mathrm{ss}}\sum_{\mu=0}^{\Theta} V_\mu^\theta\Psi_\mu(x,y)\right) = \left(\overline{V}\,\vec{c}^{\,\mathrm{ss}}\right)\cdot\vec{\Psi} \end{aligned} \tag{A65}$$

where

$$\overline{V} = \begin{bmatrix} V_0^0 & V_0^1 & \cdots & V_0^\Theta \\ V_1^0 & V_1^1 & \cdots & V_1^\Theta \\ \vdots & \vdots & \ddots & \vdots \\ V_\Theta^0 & V_\Theta^1 & \cdots & V_\Theta^\Theta \end{bmatrix} \tag{A66}$$

Similarly a single Φ_m harmonic multiplied by the velocity profile is written as:

$$\frac{1}{l}u(x,y)\Phi_m(x,y) = \sum_{\mu=0}^{\Theta} U_\mu^m\Psi_\mu(x,y), \tag{A67}$$

and thus the expression for $(1/l)u(x,y)\left(\vec{c}^{\,\mathrm{dff}}\cdot\vec{\Phi}\right)$ is:

$$\begin{aligned} \frac{1}{l}u(x,y)\left(\vec{c}^{\,\mathrm{dff}}\cdot\vec{\Phi}\right) &= \frac{1}{l}u(x,y)\sum_{m=0}^{M} c_m^{\mathrm{dff}}\Phi_m(x,y) \\ &= \sum_{m=0}^{M}\left(c_m^{\mathrm{dff}}\sum_{\mu=0}^{\Theta} U_\mu^m\Psi_\mu(x,y)\right) \\ &= \left(\widehat{U}\,\vec{c}^{\,\mathrm{dff}}\right)\cdot\vec{\Psi} \end{aligned} \tag{A68}$$

where

$$\widehat{U} = \begin{bmatrix} U_0^0 & U_0^1 & \cdots & U_0^M \\ U_1^0 & U_1^1 & \cdots & U_1^M \\ \vdots & \vdots & \ddots & \vdots \\ U_M^0 & U_M^1 & \cdots & U_M^M \\ U_{M+1}^0 & U_{M+1}^1 & \cdots & U_{M+1}^M \\ U_{M+2}^0 & U_{M+2}^1 & \cdots & U_{M+2}^M \\ \vdots & \vdots & \ddots & \vdots \\ U_{2M+1}^0 & U_{2M+1}^1 & \cdots & U_{2M+1}^M \\ & \vdots & & \\ U_{N(M+1)}^0 & U_{N(M+1)}^1 & \cdots & U_{N(M+1)}^M \\ U_{NM+N+1}^0 & U_{NM+N+1}^1 & \cdots & U_{NM+N+1}^M \\ \vdots & \vdots & \ddots & \vdots \\ U_\Theta^0 & U_\Theta^1 & \cdots & U_\Theta^M \end{bmatrix}. \tag{A69}$$

$\widehat{U}$ and all following matrices denoted with $\widehat{\ }$ are $M+1$ by $(M+1)(N+1)+1$ matrices that map from $\rightharpoonup$ vector space to the other $\vec{}$ vector space.

The $\vec{s}^{\,\mathrm{snk}}$ vector in (A63) is thus expressed as:

$$\vec{s}^{\,\mathrm{snk}} = \tilde{v}\left(\overline{V}\,\vec{c}^{\,\mathrm{ss}} + \widehat{U}\,\vec{c}^{\,\mathrm{dff}}\right) = \tilde{v}\left(\overline{V}\,\vec{c}^{\,\mathrm{ss}} + \widehat{U}\,\vec{j}\right). \tag{A70}$$

Together with (A53) this gives

$$c^{\mathrm{snk}}(x,y) = \tilde{v}\left(\overline{B}\left(\overline{V}\,\vec{c}^{\,\mathrm{ss}} + \widehat{U}\,\vec{j}\right)\right)\cdot\vec{\Psi} - c_{\mathrm{intg}} \tag{A71}$$

Due to the choice (A37) $c^{\mathrm{ss}}_{\mathrm{intg}}$ is expressed as: $c^{\mathrm{ss}}_{\mathrm{intg}} = c^{\mathrm{src}}_{\mathrm{intg}} - c^{\mathrm{snk}}_{\mathrm{intg}} = c_{\mathrm{intg}}$. Thus the first component of $\vec{c}^{\,\mathrm{ss}}$ is c_{intg}. Since $\Psi_0 = 1$ is also the first component of $\vec{\Psi}$ the constant term c_{intg} in (A71) can be expressed as:

$$c_{\mathrm{intg}} = \left(\overline{0}^{1}\vec{c}^{\,\mathrm{ss}}\right)\cdot\vec{\Psi} \tag{A72}$$

where

$$\overline{0}^{1} = \begin{bmatrix} 1 & 0 & \cdots & 0 \\ 0 & 0 & \cdots & 0 \\ \vdots & \vdots & \ddots & \vdots \\ 0 & 0 & \cdots & 0 \end{bmatrix}. \tag{A73}$$

Using this the Equation (A71) becomes:

$$\begin{aligned} c^{\mathrm{snk}}(x,y) &= \left(\left(\tilde{v}\overline{BV} - \overline{0}^{1}\right)\vec{c}^{\,\mathrm{ss}} + \tilde{v}\overline{B}\widehat{U}\,\vec{j}\right)\cdot\vec{\Psi} \\ &= \left(\left(\tilde{v}\overline{\Omega} - \overline{0}^{1}\right)\vec{c}^{\,\mathrm{ss}} + \tilde{v}\widehat{F}\,\vec{j}\right)\cdot\vec{\Psi}, \end{aligned} \tag{A74}$$

where

$$\overline{\Omega} = \overline{BV}, \quad \widehat{F} = \overline{B}\widehat{U} \tag{A75}$$

and (A61) becomes:

$$\begin{aligned} c^{\mathrm{ss}}(x,y) &= \vec{c}^{\,\mathrm{ss}}\cdot\vec{\Psi} + c^{\mathrm{ss}}_{t}t \\ &= \left(\overline{B}\,\vec{s}^{\,\mathrm{src}}\right)\cdot\vec{\Psi} - \left(\left(\tilde{v}\overline{\Omega} - \overline{0}^{1}\right)\vec{c}^{\,ss} + \tilde{v}\widehat{F}\,\vec{j}\right)\cdot\vec{\Psi} \end{aligned} \tag{A76}$$

From definition (A61) and condition (A42) it follows that: $c^{\mathrm{ss}}_{t} = c^{\mathrm{src}}_{t} - c^{\mathrm{snk}}_{t} = -c^{\mathrm{dff}}_{t} = -\omega j_0 t$. In similar fashion as in expression (A72) the term $\omega j_0 t$ can be expressed as:

$$\omega j_0 t = \omega j_0 t\Psi_0 = \left(\widehat{0}^{\,\omega t}\,\vec{j}\right)\cdot\vec{\Psi}, \tag{A77}$$

where

$$\widehat{0}^{\,\omega t} = \begin{bmatrix} \omega t & 0 & \cdots & 0 \\ 0 & 0 & \cdots & 0 \\ \vdots & \vdots & \ddots & \vdots \\ 0 & 0 & \cdots & 0 \\ & \vdots & & \\ 0 & 0 & \cdots & 0 \\ 0 & 0 & \cdots & 0 \\ \vdots & \vdots & \ddots & \vdots \\ 0 & 0 & \cdots & 0 \end{bmatrix} \tag{A78}$$

Together with Equation (A76) this gives:

$$\begin{aligned} \vec{c}^{\,\mathrm{ss}}\cdot\vec{\Psi} &= \left(\overline{B}\,\vec{s}^{\,\mathrm{src}}\right)\cdot\vec{\Psi} - \left(\left(\tilde{v}\overline{\Omega} - \overline{0}^{1}\right)\vec{c}^{\,\mathrm{ss}} + \tilde{v}\widehat{F}\,\vec{j}\right)\cdot\vec{\Psi} \\ &\quad - \left(\widehat{0}^{\,\omega t}\,\vec{j}\right)\cdot\vec{\Psi} \Rightarrow \vec{c}^{\,\mathrm{ss}} \\ &= \overline{B}\,\vec{s}^{\,\mathrm{src}} - \left(\tilde{v}\overline{\Omega} - \overline{0}^{1}\right)\vec{c}^{\,\mathrm{ss}} - \left(\tilde{v}\widehat{F} - \widehat{0}^{\,\omega t}\right)\vec{j}, \end{aligned} \tag{A79}$$

rearranging:

$$\overline{B}\,\vec{s}^{\,\mathrm{src}} - \left(\overline{1}^{0} + \tilde{v}\overline{\Omega}\right)\vec{c}^{\,\mathrm{ss}} - \left(\tilde{v}\widehat{F} - \widehat{0}^{\,\omega t}\right)\vec{j} = 0 \tag{A80}$$

where $\overline{1}^{0} = \overline{1} - \overline{0}^{1}$ with $\overline{1}$ being identity matrix.

The upper Equation (A80) also contains the steady state condition (A42). This can be verified by inspecting the first components of all the terms in this equation: Following definitions (A51) and (A52) the first component of $\overline{B}\,\vec{s}^{\,\mathrm{src}}$ is $ts^{\mathrm{src}}_{0} = tc^{\mathrm{src}}_{t}$, following definitions (A23), (A35) and (A69) the first component of $\widehat{0}^{\,\omega t}\,\vec{j}$ is $\omega j_0 t = tc^{\mathrm{dff}}_{t}$, first component of $\overline{1}^{0}\vec{c}^{\,\mathrm{ss}}$ is zero and, due to Equations (A70) and (A75) the remaining term is $\tilde{v}\overline{\Omega}\,\vec{c}^{\,\mathrm{ss}} - \tilde{v}\widehat{F}\,\vec{j} = \overline{B}\tilde{v}(\overline{V}\,\vec{c}^{\,\mathrm{ss}} + \widehat{U}\,\vec{j}\,) = \overline{B}\,\vec{s}^{\,\mathrm{snk}}$ with its first component being $ts^{\mathrm{snk}}_{0} = tc^{\mathrm{snk}}_{t}$. All these first components sum up to:

$$ts^{\mathrm{src}}_{0} - ts^{\mathrm{snk}}_{0} + \omega j_0 t = t\left(c^{\mathrm{src}}_{t} - c^{\mathrm{snk}}_{t} + c^{\mathrm{dff}}_{t}\right) = 0 \tag{A81}$$

By means of eigen functions the differential Equation (8) has been translated into an algebraic Equation (A80) which is the partial solution for gas element. For a complete solution for a slice coupling of the two gas and the membrane elements and 1D gas flow equations are needed.

A.2. Membrane element

In this section the diffusion equation for water transport in membrane is expressed in the vector notation introduced in the previous subsection.

The membrane water content at the boundary with cathode element $\Lambda^{\mathrm{O}}(y)$ and anode element $\Lambda^{\mathrm{H}}(y)$ is assumed to be in equilibrium with the concentration of water vapour at the membrane-element boundary $c(x = h, y)$.

Let us define another variable $\zeta(y) \equiv c(x = h, y)$. With this Equation (20) reads:

$$\Lambda^{\mathrm{O}}(y) - \Lambda^{\mathrm{H}}(y) = \chi\left(\zeta^{\mathrm{O}}(y) - \zeta^{\mathrm{H}}(y)\right), \tag{A82}$$

where ζ^{O} and ζ^{H} are the ζ on the cathode side and anode side respectively. Equation (16) thus becomes:

$$j_{\mathrm{H}}(y) = D_{\mathrm{mmb}}\frac{\chi}{q}\left(\zeta^{\mathrm{O}}(y) - \zeta^{\mathrm{H}}(y)\right) - n_{\mathrm{drg}}\frac{i(y)}{F} \tag{A83}$$

$i(y)$ in vector notation is expressed as:

$$i(y) = \sum_{m=0}^{M} i_m \cos\left(\frac{m\pi}{w}y\right) = \vec{i}\cdot\vec{\cos}\,, \tag{A84}$$

$$\vec{i} = (i_0, i_1, i_2, \ldots, i_M)^{T}, \tag{A85}$$

$\zeta(y)$ in vector notation is expressed as:

$$\begin{aligned}\zeta(y) &= c(x=h,y) = \sum_{m,n} c^{ss}_{m,n}\Psi_{m,n}(x=h,y) \\ &+ \sum_{m} c^{dff}_{m}\Phi_{m}(x=h,y) = \sum_{m,n} c^{ss}_{m,n}\cos\left(\frac{m\pi}{w}y\right) \\ &+ \sum_{m} c^{dff}_{m}(a_m+b_m)\cos\left(\frac{m\pi}{w}y\right) = \sum_{\theta=0}^{\Theta} c^{ss}_{\theta}\cos\left(\frac{m(\theta)\pi}{w}y\right) \\ &+ \sum_{m=0}^{M} c^{dff}_{m}(a_m+b_m)\cos\left(\frac{m\pi}{w}y\right) = \left(\check{G}\vec{c}^{ss}\right)\cdot\vec{\cos} \\ &+ \left(\underline{H}\,\vec{c}^{dff}\right)\cdot\vec{\cos} = \left(\vec{\zeta}^{ss}+\vec{\zeta}^{dff}\right)\cdot\vec{\cos} = \vec{\zeta}\cdot\vec{\cos} \end{aligned} \quad (A86)$$

where

$$\vec{\zeta} = (\zeta_0,\zeta_1,\zeta_2,\ldots,\zeta_M)^T \quad (A87)$$

$$\underline{H} = \begin{bmatrix} 0 & 0 & \cdots & 0 \\ 0 & a_1+b_1 & \cdots & 0 \\ \vdots & \vdots & \ddots & \vdots \\ 0 & 0 & \cdots & a_M+b_M \end{bmatrix} \quad (A88)$$

$$\check{G} = \left[\begin{array}{cccccccc|c|cccc} 1 & 0 & \cdots & 0 & 1 & 0 & \cdots & 0 & & 1 & 0 & \cdots & 0 \\ 0 & 1 & \cdots & 0 & 0 & 1 & \cdots & 0 & \cdots & 0 & 1 & \cdots & 0 \\ \vdots & \vdots & \ddots & \vdots & \vdots & \vdots & \ddots & \vdots & & \vdots & \vdots & \ddots & \vdots \\ 0 & 0 & \cdots & 1 & 0 & 0 & \cdots & 1 & & 0 & 0 & \cdots & 1 \end{array}\right] \quad (A89)$$

$\underline{H}$ and all following matrices denoted with _ are $M+1$ by $M+1$ matrices that map from $\rightharpoonup$ vector space to the same $\rightharpoonup$ vector space. $\check{G}$ is a $(M+1)(N+1)$ by $M+1$ matrix that maps from $\rightharpoonup$ vector space to the other$\rightharpoonup$ vector space.

Using expressions (A23), (A59), (A84) and (A78) the diffusion equation for membrane (A83) is expressed in following vector notation:

$$\begin{aligned}\vec{j}_{\mathrm{H}} &= D_{\mathrm{mmb}}\chi\frac{\left(\vec{\zeta}_{\mathrm{O}}-\vec{\zeta}_{\mathrm{H}}\right)}{q} - n_{\mathrm{drg}}\frac{\vec{i}}{F} \\ &= D_{\mathrm{mmb}}\frac{\chi}{q}\left(\check{G}(\vec{c}^{ss}_{\mathrm{O}}-\vec{c}^{ss}_{\mathrm{H}})+\underline{H}\left(\vec{j}_{\mathrm{O}}-\vec{j}_{\mathrm{H}}\right)\right) - n_{\mathrm{drg}}\frac{\vec{i}}{F}\end{aligned} \quad (A90)$$

where O and H in super- or subscript denote the cathode and anode side respectively. To account for the nonlinearity in Λ to c dependence the constant χ is to be modified in the following way:

$$\chi = \frac{\Lambda\left(\zeta^{\mathrm{O}}_0\right)-\Lambda\left(\zeta^{\mathrm{H}}_0\right)}{\zeta^{\mathrm{O}}_0-\zeta^{\mathrm{H}}_0} \quad (A91)$$

where ζ^{O}_0 and ζ^{H}_0 are the first component of vectors $\vec{\zeta}^{\mathrm{O}}$ and $\vec{\zeta}^{\mathrm{H}}$. Considering the expression $\zeta(y) = \vec{\zeta}\cdot\vec{\cos}$ and acknowledging that the first component of $\vec{\cos}$ is the constant 1 while all other components have average of zero it is evident that the first component of $\vec{\zeta}$ i.e. ζ_0 is exactly the average of $\zeta(y)$. Thus ζ^{O}_0 and ζ^{H}_0 are the average of $\zeta(y)$ on the oxygen and hydrogen side respectively. The nonlinear function $\Lambda = \Lambda(\zeta_0)$ is obtained by combining Equations (17) and (18). In the calculation χ is iteratively corrected using ζ^{O}_0 and ζ^{H}_0 from previous iteration.

Using (A91) in (A90) neglects nonlinear effects of the deviations from the average. This is justifiable since these deviations are small as can be seen in Figs. 11 and 12.

A.3. Solution for a slice

Using the presented vector notation the governing equations for the two gas elements and the membrane element are transformed into the following algebraic equations that give the solution for a slice:

The continuity condition (15) in vector notation reads:

$$j_{\mathrm{O}}(y)+j_{\mathrm{H}}(y) = \frac{i(y)}{2F} \Rightarrow \vec{j}_{\mathrm{H}}+\vec{j}_{\mathrm{O}} = \frac{\vec{i}}{2F} \quad (A92)$$

All together the 2D analytic partial solutions of the diffusion equation resulting in Equations (A80), (A90) and (A92) form the following system of four linear algebraic equations dealing with the four unknowns $\vec{c}^{ss}_{\mathrm{O}}$, $\vec{c}^{ss}_{\mathrm{H}}$, $\vec{j}_{\mathrm{O}}$ and $\vec{j}_{\mathrm{H}}$:

$$\begin{aligned} &\overline{B}_{\mathrm{H}}\vec{s}^{src}_{\mathrm{H}} - \left(\tilde{\nu}_{\mathrm{H}}\overline{\Omega}_{\mathrm{H}}+\overline{1}^0\right)\vec{c}^{ss}_{\mathrm{H}} - \left(\tilde{\nu}_{\mathrm{H}}\widehat{F}_{\mathrm{H}}-\widehat{0}^{\omega t}\right)\vec{j}_{\mathrm{H}} = 0 \\ &\overline{B}_{\mathrm{O}}\vec{s}^{src}_{\mathrm{O}} - \left(\tilde{\nu}_{\mathrm{O}}\overline{\Omega}_{\mathrm{O}}+\overline{1}^0\right)\vec{c}^{ss}_{\mathrm{O}} - \left(\tilde{\nu}_{\mathrm{O}}\widehat{F}_{\mathrm{O}}-\widehat{0}^{\omega t}\right)\vec{j}_{\mathrm{O}} = 0 \\ &\vec{j}_{\mathrm{H}} = D_{\mathrm{mmb}}\chi\left(\check{G}(\vec{c}^{ss}_{\mathrm{O}}-\vec{c}^{ss}_{\mathrm{H}})+\underline{H}\left(\vec{j}_{\mathrm{O}}-\vec{j}_{\mathrm{H}}\right)\right) - n_{\mathrm{drg}}\frac{\vec{i}}{F} \\ &\vec{j}_{\mathrm{H}}+\vec{j}_{\mathrm{O}} = \frac{\vec{i}}{2F} \end{aligned} \quad (A93)$$

The remaining three unknowns χ, $\tilde{\nu}_{\mathrm{H}}$ and $\tilde{\nu}_{\mathrm{O}}$, which are nonlinear functions of $\vec{c}^{ss}_{\mathrm{O}}$, $\vec{c}^{ss}_{\mathrm{H}}$, $\vec{j}_{\mathrm{O}}$ and $\vec{j}_{\mathrm{H}}$, are, within the set of Equation (A93), treated as parameters. They are calculated separately: χ by Equations (17) and (18) and (A91); and $\tilde{\nu}_{\mathrm{H}}$ and $\tilde{\nu}_{\mathrm{H}}$ by the equations of 1D gas flow (described in the following section). All these linear and nonlinear calculations are repeatedly performed in the iterative routine as described in Section 3.3.

A.4. Equations of 1D gas flow

The scalar variables of 1D gas-flow are: the total molar flux of gas $\dot{n}$, the total mass flux of gas $\dot{m}$, flux of linear momentum $\dot{L}$, pressure p and velocity $\tilde{v}$. For all these the following general equation applies:

$$X = X_{\mathrm{pr}} + \Delta X \quad (A94)$$

where X can be any of the aforementioned scalar variables. X_{pr} is the value on the boundary between the current element and its' upstream neighbour element and X is the value on the boundary between the current element and its' downstream neighbour element. The steady state momentum equation for the channel region of a gas element (22) is:

$$-wd\Delta p + F_{fr} = \Delta\dot{L}, \quad (A95)$$

where $wd = A$ represent the cross-sectional area of the channel.

The friction force between the gas and the channel walls of the gas element F_{fr} is expressed as:

$$F_{fr} = -\eta l \oint_{\partial(d^*w)} \frac{\partial v(x,y)}{\partial n} \mathrm{d}s \tag{A96}$$

where η is the coefficient of viscosity, $\partial(d^*w)$ denotes the edge of the d by w rectangle of the channel cross-section and n direction normal to the wall. The integral in (A96) expresses as:

$$\oint_{\partial(d^*w)} \frac{\partial v(x,y)}{\partial n} \mathrm{d}s = \int_0^w (\partial_x v|_{x=0} - \partial_x v|_{x=d}) \mathrm{d}y + \int_0^d \left(\partial_y v|_{y=0} - \partial_y v|_{y=w}\right) \mathrm{d}x \tag{A97}$$

Given the velocity profile v derived in Appendix B the upper integrals evaluate to:

$$\int_0^w (\partial_x v|_{x=0} - \partial_x v|_{x=d})\ \mathrm{d}y + \int_0^d \left(\partial_y v|_{y=0} - \partial_y v|_{y=w}\right)\ \mathrm{d}x = \frac{\tilde{\nu}}{\tilde{u}} \frac{2w}{d} \equiv \tilde{\nu} \frac{\sigma_{fr}}{l} \tag{A98}$$

where the geometric friction factor is defined as: $\sigma_{fr} \equiv (2wl/\tilde{u}d)$. The friction force is thus simply expressed as:

$$F_{fr} = -\eta \tilde{\nu} \sigma_{fr} \tag{A99}$$

The change in linear momentum flux takes into account the change in velocity $\Delta\tilde{\nu}$ and the change in mass flow $\Delta\dot{m}$ giving:

$$\Delta \dot{L} = \tilde{\nu}_{\mathrm{pr}} \Delta \dot{m} + \Delta\tilde{\nu}(\Delta \dot{m} + \dot{m}_{\mathrm{pr}}) \tag{A100}$$

Using the ideal gas equation in the form:

$$p\tilde{\nu} wd = \dot{n} RT \tag{A101}$$

$\Delta\tilde{\nu}$ and Δp are expressed as

$$\begin{aligned} \Delta\tilde{\nu} &= \frac{\Delta \dot{n}_{\mathrm{pr}} RT - \tilde{\nu}_{\mathrm{pr}}^2 \left(wd\eta\sigma_{fr} + \Delta\dot{m}\right)}{wdp_{\mathrm{pr}} - \tilde{\nu}_{\mathrm{pr}}\left(\dot{m}_{\mathrm{pr}} + \Delta\dot{m} + 0.5wd\eta\sigma_{fr}\right)} \\ \Delta p &= -\left(\left(\tilde{\nu}_{\mathrm{pr}} + \frac{\Delta\tilde{\nu}}{2}\right)\eta\sigma_{fr} + \frac{(\tilde{\nu}_{\mathrm{pr}} + \Delta\tilde{\nu})\Delta\dot{m} + \Delta\tilde{\nu}\dot{m}}{wd}\right) \end{aligned} \tag{A102}$$

The changes in molar flow and mass flow are governed by consumption of reactants on the catalyst and diffusion of water from the membrane into gas element. These are for the cathode gas element (denoted with sub- or superscript O) and anode gas element (denoted with sub- or superscript H) as follows:

The molar consumption of oxygen (O_2) on the cathode catalyst within one slice takes place at a rate of $wl(i_0/2F)$ and the molar flow of water from membrane to the cathode gas element is wlj_0^{O}, where wl is the area of the boundary between gas element and membrane element and, following the rationale under Equation (A91), i_0 and j_0^{O} represent the average of $i(y)$ and $j^{\mathrm{O}}(y)$. This gives for the cathode gas element:

$$\Delta \dot{n}_{\mathrm{O}} = wl\left(j_0^{\mathrm{O}} - \frac{i_0}{4F}\right), \tag{A103}$$

$$\Delta \dot{m}_{\mathrm{O}} = wl\left(M(\mathrm{H_2O})j_0^{\mathrm{O}} - M(\mathrm{O_2})\frac{i_0}{4F}\right), \tag{A104}$$

where $M(H_2O)$ and $M(O_2)$ are molar masses of water and oxygen respectively. Similar equations apply for anode gas element where hydrogen with molar mass $M(H_2)$ is consumed at the rate of $wl(i_0/F)$:

$$\Delta \dot{n}_{\mathrm{H}} = wl\left(j_0^{\mathrm{H}} - \frac{i_0}{2F}\right) \tag{A105}$$

$$\Delta \dot{m}_{\mathrm{H}} = wl\left(M(\mathrm{H_2O})j_0^{\mathrm{H}} - M(\mathrm{H_2})\frac{i_0}{2F}\right) \tag{A106}$$

Appendix B

Derivation of velocity profile:

The partial differential equation for velocity profile of a viscid flow in a straight channel stretching along z axis reads:

$$\left(\frac{\partial^2}{\partial^2 x} + \frac{\partial^2}{\partial^2 y}\right) v = \frac{1}{\eta}\frac{\partial p}{\partial z} = \frac{\Delta p}{\eta l}, \tag{B1}$$

where Δp is pressure difference between two consecutive elements. The ansatz for a channel with d by w rectangular cross-section that solves the upper partial differential equation is:

$$\begin{aligned} v(x,y) &= -\frac{2\Delta p}{\eta l d^2}\left(\frac{x}{d} - \frac{x^2}{d^2} - \sum_{n=1}^{\infty} a_i \sin\left(\frac{n\pi}{d}x\right)\cosh\left(\frac{n\pi}{d}\left(\frac{w}{2} - y\right)\right)\right) \\ &= \tilde{\nu}\frac{\vartheta(x,y)}{\tilde{\vartheta}} \equiv \tilde{\nu} u(x,y) \end{aligned} \tag{B2}$$

where $\tilde{v}$ is the average velocity of the gas in the channel within the gas element, $\tilde{\vartheta} = (1/dw)\int_0^d \int_0^w \vartheta(x,y)\mathrm{d}x\mathrm{d}y$ and $-(2\Delta p/\eta l d^2) = \tilde{v}/\tilde{\vartheta}$. This ansatz also satisfies the boundary condition: $v(x = 0, y) = v(x = d, y) = 0$. By appropriate choice of a_i coefficients also the other boundary condition $v(x, y = 0) = v(x, y = w) = 0$ can be met. To find these a_i coefficients first let us find coefficients b_i for Fourier sin series of $(x/d) - (x^2/d^2)$ on $x \in [0, d]$:

$$\frac{x}{d} - \frac{x^2}{d^2} = \sum_{n=1}^{\infty} b_i \sin\left(\frac{n\pi}{d}x\right) \Rightarrow b_i = \begin{cases} \frac{8}{n^3\pi^3} & \text{for } n \text{ odd} \\ 0 & \text{for } n \text{ even} \end{cases} \tag{B3}$$

By setting $y = 0$ or $y = w$ in Equation (B2) the appropriate choice for a_i coefficients is identified as: $a_i = b_i/\cosh((n\pi/d)(w/2))$. By defining $n = 2k + 1$ and taking into account assumption X the full expression for $\vartheta(x, y)$ reads:

$$\vartheta(x,y) = \begin{cases} \frac{x}{d}\left(1 - \frac{x}{d}\right) - \sum_{k=0}^{\infty} \frac{8\sin\left(\frac{(2k+1)\pi}{d}x\right)\cosh\left(\frac{(2k+1)\pi}{d}\left(y - \frac{w}{2}\right)\right)}{(2k+1)^3\pi^3\cosh\left(\frac{(2k+1)\pi}{d}\frac{w}{2}\right)} & x < d \\ 0 & d < x < h \end{cases} \tag{B4}$$

Appendix C

Calculation of $k_{1,m,n}$, $k_{2,m,n}$ and $\gamma_{m,n}$ from (A16):

Operator $D\nabla^2$ acting on $\Psi_{m,n}$ gives (D takes on value D_{GDL} in the GDL and D_{chnl} in the channel):

$$D\nabla^2\Psi_{m,n}(x,y) = \lambda_{m,n}\Psi_{m,n}(x,y) = \begin{cases} D_{\mathrm{GDL}}\left(\left(\frac{m\pi}{w}\right)^2 + k_{1,m,n}^2\right)\Psi_{m,n}(x,y) & x\in \mathrm{GDL} \\ D_{\mathrm{chnl}}\left(\left(\frac{m\pi}{w}\right)^2 + k_{2,m,n}^2\right)\Psi_{m,n}(x,y) & x\in \mathrm{channel} \end{cases} \tag{C1}$$

The fact that $\Psi_{m,n}$ has a well defined eigen value $\lambda_{m,n}$ thus requires that:

$$D_{\mathrm{GDL}}\left(\left(\frac{m\pi}{w}\right)^2 + k_{1,m,n}^2\right) = D_{\mathrm{chnl}}\left(\left(\frac{m\pi}{w}\right)^2 + k_{2,m,n}^2\right) \tag{C2}$$

The continuity of $\Psi_{m,n}$ requires that:

$$\cos\left(k_{1,m,n}(h-d)\right) = \gamma_{m,n}\cos\left(k_{2,m,n}d\right) \tag{C3}$$

And continuity equation for flux between GDL and channel requires that:

$$\begin{aligned} j_{\mathrm{GDL}}|_{x=d} = j_{\mathrm{chnl}}|_{x=d} &\Rightarrow \kappa D_{\mathrm{GDL}}\left.\frac{\partial\Psi_{m,n}}{\partial x}\right|_{x=d^+} = D_{\mathrm{chnl}}\left.\frac{\partial\Psi_{m,n}}{\partial x}\right|_{x=d^-} \\ &\Rightarrow \kappa D_{\mathrm{GDL}}k_{1,m,n}\sin\left(k_{1,m,n}(h-d)\right) \\ &= D_{chnl}\gamma_{m,n}k_{2,m,n}\sin\left(k_{2,m,n}d\right) \end{aligned} \tag{C4}$$

The obtained 3 Equations (C 2), (C 3) and (C 4) are solved numerically (e.g. bisection) due to their transcendent nature.

Appendix D

Calculation of a_m, b_m, and α_m from (A27).

Condition (A21) together with definition (A26) requires that:

$$\kappa D_{\mathrm{GDL}}\left.\frac{\partial \mathrm{HYPTRG}_m(x)}{\partial x}\right|_{x=h} = \kappa D_{\mathrm{GDL}}\frac{m\pi}{w}(a_m - b_m) = 1 \tag{D1}$$

the continuity requires that:

$$a_m e^{\frac{m\pi}{w}(h-d)} + b_m e^{-\frac{m\pi}{w}(h-d)} = \alpha_m\cosh\left(\frac{m\pi}{w}d\right) \tag{D2}$$

And continuity of flux between GDL and channel requires that:

$$\begin{aligned} j_{\mathrm{GDL}}|_{x=d} = j_{\mathrm{chnl}}|_{x=d} &\Rightarrow \kappa D_{\mathrm{GDL}}\left.\frac{\partial \mathrm{HYPTRG}_m(x)}{\partial x}\right|_{x=d^+} \\ &= D_{chnl}\left.\frac{\partial \mathrm{HYPTRG}_m(x)}{\partial x}\right|_{x=d^-} \Rightarrow \kappa D_{\mathrm{GDL}}\left(a_m e^{\frac{m\pi}{w}(h-d)} - b_m e^{-\frac{m\pi}{w}(h-d)}\right) \\ &= D_{\mathrm{chnl}}\alpha_m\sinh\left(\frac{m\pi}{w}d\right) \end{aligned} \tag{D3}$$

altogether giving:

$$\begin{aligned} a_m &= \frac{w}{\kappa D_{\mathrm{GDL}}m\pi\left(\frac{e^{\frac{2m\pi}{w}(h-d)}\left(D_{\mathrm{chnl}}\sinh\left(\frac{m\pi}{w}d\right) - \kappa D_{\mathrm{GDL}}\cosh\left(\frac{m\pi}{w}d\right)\right)}{D_{\mathrm{chnl}}\sinh\left(\frac{m\pi}{w}d\right) + \kappa D_{\mathrm{GDL}}\cosh\left(\frac{m\pi}{w}d\right)} + 1\right)} \\ b_m &= \frac{w}{\kappa D_{\mathrm{GDL}}m\pi\left(\frac{e^{\frac{2m\pi}{w}(h-d)}\left(D_{\mathrm{chnl}}\sinh\left(\frac{m\pi}{w}d\right) + \kappa D_{\mathrm{GDL}}\cosh\left(\frac{m\pi}{w}d\right)\right)}{D_{\mathrm{chnl}}\sinh\left(\frac{m\pi}{w}d\right) - \kappa D_{\mathrm{GDL}}\cosh\left(\frac{m\pi}{w}d\right)} - 1\right)} \\ \alpha_m &= \frac{w}{m\pi\left(D_{\mathrm{chnl}}\cosh\left(\frac{m\pi}{w}(h-d)\right)\sinh\left(\frac{m\pi}{w}d\right) - \kappa D_{\mathrm{GDL}}\cosh\left(\frac{m\pi}{w}d\right)\sinh\left(\frac{m\pi}{w}(h-d)\right)\right)} \end{aligned} \tag{D4}$$

References

[1] Denver Cheddie, Norman Munroe, J. Power Sources 147 (2005) 1–2.
[2] Kristina Haraldsson, Keith Wipke, J. Power Sources 126 (2003) 1–2.
[3] M. Usman Iftikar, et al., J. Power Sources 160 (2006) 2.
[4] R. Tirnovan, et al., Int. J. Hydrogen Energy 33 (2008) 21.
[5] X.D. Xue, K.W.E. Cheng, D. Sutanto, Electrochim. Acta 52 (2006) 3.
[6] T.E. Springer, T.A. Zawodzinski, S. Gottesfeld, J. Electrochem. Soc. 138 (1991) 8.
[7] M. Wohr, et al., Int. J. Hydrogen Energy 23 (1998) 3.
[8] G. Maggio, V. Recupero, L. Pino, J. Power Sources 101 (2001) 2.
[9] Vladimir Gurau, Frano Barbir, Hongtan Liu, J. Electrochem. Soc. 147 (2000) 7.
[10] J.J. Baschuk, Li Xianguo, Appl. Energy 86 (2009) 2.
[11] B.P.M. Rajani, Ajit Kumar Kolar, J. Power Sources 164 (2007) 1.
[12] M. Khakbaz Baboli, M.J. Kermani, Electrochim. Acta 53 (2008) 26.
[13] Hua Meng, J. Power Sources 162 (2006) 1.
[14] B.R. Sivertsen, N. Djilali, J. Power Sources 141 (2005) 1.
[15] Andreas Vath, et al., J. Power Sources 157 (2006) 2.
[16] M.A.R.S. Al-Baghdadi, H.A.K.S. Al-Janabi, Proc. IMechE 221 (2007).
[17] Fabian Mueller, et al., J. Power Sources 163 (2007) 2.
[18] R. Tirnovan, et al., J. Power Sources 175 (2008) 2.
[19] Mustapha Hatti, Mustapha Tioursi, Int. J. Hydrogen Energy 34 (2009) 11.
[20] Peter Berg, et al., J. Electrochem. Soc. 151 (2004) 3.
[21] AVL, AVL FIRE Version 2011 User Manual, Document No. 08.0205.2011: Electrification & Hybridization, AVL LIST GmbH, Graz, 2011.
[22] M.A.R.S. Al-Baghdadi, Proc. IMechE 222 (2008).
[23] Edward Lansing Cussler, Diffusion: Mass Transfer in Fluid Systems 3rd Edition, Cambridge University Press, Cambridge, 2009.
[24] Desmond E. Winterbone, Richard J. Pearson, Theory of Engine Manifold Design, Society of Automotive Engineers, Inc., Warrendale, 2000.
[25] Clemens Fink, Nicolas Fouquet, Electrochim. Acta 56 (2011) 28.
[26] Fouquet Nicolas, Fink Clemens, Tatschl Reinhard, 3D Modeling of PEM Fuel Cell with AVL FIRE, AVL Advanced Simulation Technologies International User Conference 2011, Graz, 2011.

Glossary

Symbols

$\bar{0}^{-1}$: matrix defined in Equation (A73)
$\hat{0}^{\omega t}$: matrix defined in Equation (A78)
A: channel cross-sectional area
a_m: coefficients for Φ_m defined in Appendix D

$\overline{B}$: matrix defined in Equation (A52)
b_m: coefficients for Φ_m defined in Appendix D
c: water vapour concentration
D: diffusion constant
d: channel height
F: Faraday constant
F_{fr}: friction force between gas flow and channel walls
$\tilde{G}$: matrix defined in Equation (A89)
$\underline{H}$: matrix defined in Equation (A88)
h: sum of channel height and GDL thickness
i: electric/proton current density
j: molar flux of water
$k_{1,m,n}$, $k_{2,m,n}$: wave vectors
l: depth of slice
$\dot{L}$: flux of linear momentum
M: maximal number of harmonics in y coordinate
m: harmonics index in y coordinate
$\dot{m}$: mass flux
N: maximal number of harmonics in x coordinate
n: coordinate normal to boundary plane, harmonics index in x coordinate
$\dot{n}$: molar flux
n_{drg}: electroosmotic drag coefficient
p: pressure
p_0: ambient pressure
q: membrane thickness
R: gas constant
$\underline{Rh}$: relative humidity
$\overline{Rh}$: relative humidity averaged over y coordinate
δRh: deviation of ^{Rh} from $\widetilde{\overline{Rh}}$
s: source/sink term
t: time
T: temperature
u: dimensionless shape of velocity profile
$\hat{U}$: matrix defined in Equation (A69)
v: velocity
$\bar{v}$: average velocity
$\overline{V}$: matrix defined in Equation (A66)
w: width of channel/GDL
x: coordinate perpendicular to membrane
y: coordinate along channel/GDL width
z: coordinate along fuel cell length (direction of gas-flow)

Greek letters
α_m: coefficients for Φ_m defined in Appendix D
β_m: coefficients for Φ_m defined in Appendix D
$\gamma_{m,n}$: coefficients for $\Psi_{m,n}$ defined in Appendix C
Δ: change of variable along depth of slice
ζ: water vapour concentration at membrane
η: dynamic viscosity
Θ: maximal value of θ
θ: counter of m, n double index
κ: volume fraction of non-solid space in GDL
Λ: membrane water content
$\lambda_{m,n}$: eigen value of $\Psi_{m,n}$
ξ: integration constant
σ_{fr}: geometric friction factor
Φ_m: eigen functions for diffusive flow from membrane
χ: ratio between membrane water content and water vapour concentration
$\Psi_{m,n}$: eigen functions for convective terms
ω: geometrical factor

Subscripts or superscripts
chnl: channel
cnv: convective contribution (either snk or src)
dff: contribution from diffusion from membrane
GDL: gas diffusion layer
H: anode (hydrogen) side
intg: integration constant
mmb: membrane
m, n and θ: harmonics indices
O: cathode (oxygen) side
pr: previous (upstream)
snk: sink
src: source
t: temporal term